Word count 10,400 Revised Version #2

Single-Crystal UV/Vis Absorption Spectroscopy of Aluminosilicate Garnet: Part III. $\{Fe^{2+}\} + [Fe^{3+}] \rightarrow \{Fe^{3+}\} + [Fe^{2+}]$ Intervalence Charge Transfer

Charles A. Geiger[1,2,*] and Michail N. Taran[3]

[1] Department of Chemistry and Physics of Materials
University of Salzburg
Jakob Haringer Str. 2a
A-5020 Salzburg, Austria

[2] Institute for Mineralogy and Crystallography
University of Vienna
Josef-Holaubek-Platz 2 (UZA II)
A-1090 Vienna, Austria

[3] M.P. Semenenko Institute of Geochemistry and Mineralogy and Ore Formation
National Academy of Sciences of Ukraine
Palladin Ave. 34
03680 Kyiv-142, Ukraine

[*] Corresponding author
Fax: ++43-662-8044-6289
Tel.: ++43-662-8044-6226
E-mail: charles.geiger@univie.ac.at

Revised version submitted to Am Min 29.09.22

This is the peer-reviewed, final accepted version for American Mineralogist, published by the Mineralogical Society of America.
The published version is subject to change. Cite as Authors (Year) Title. American Mineralogist, in press.
DOI: https://doi.org/10.2138/am-2022-8756. http://www.minsocam.org/

ABSTRACT

The various intervalence charge transfer (IVCT) mechanisms that can occur in silicate garnet, general crystal-chemical formula $\{X_3\}[Y_2](Z_3)O_{12}$, are not fully understood. The single-crystal UV/Vis/NIR absorption spectra of two different almandine-rich, spessartine-rich and grossular-rich garnets, as well as an intermediate almandine-pyrope garnet, were measured. Absorption was observed from roughly 15000 to 30000 cm^{-1}. The spectra were deconvoluted and a very broad band with FWHM values ranging from 5000 to 7000 cm^{-1} (except in the case of one grossular where the FWHM is 8700 cm^{-1}) and having an intensity maximum located between about 20000 and 22000 cm^{-1} in the visible region could be fit. Small weaker features located on this broad band were fit as well. The broad band is strongest in a nearly end-member composition almandine and weakest in a very grossular-rich iron-poor crystal. It is assigned to $\{Fe^{2+}\} + [Fe^{3+}] \rightarrow \{Fe^{3+}\} + [Fe^{2+}]$ IVCT. This is the first recognition of this type of electronic transition mechanism in different aluminosilicate garnet species. Photon-induced electron transfer probably occurs through an overlap of the *d* orbitals of Fe^{2+} and Fe^{3+} in their edge-shared triangular dodecahedral and octahedral coordination polyhedra, respectively. The two Fe cations with different formal charges should have markedly different energy potentials giving rise to asymmetric IVCT behavior. This, together with the relatively long Fe^{2+}-Fe^{3+} distances (greater than 3.2 Å), could explain the higher energy of the IVCT in garnet compared to $Fe^{2+} + Fe^{3+} \rightarrow Fe^{3+} + Fe^{2+}$ IVCT mechanisms observed in other minerals. The latter typically have iron cations in octahedral or quasi-octahedral coordination. The IVCT in aluminosilicate garnet can occur in different species that grew under dissimilar *P*-*T*-*X* conditions. The resulting electronic absorption band affects color markedly, because it is centered at higher energies in the blue visible region. It remains to be determined why IVCT is observed in the spectra of some garnets but not others. The various proposed IVCT mechanisms in Ca-Ti-bearing and aluminosilicate garnets are reviewed and analyzed.

Keywords: Garnet, UV/Vis absorption spectroscopy, IVCT, electronic transitions, iron, titanium.

This is the peer-reviewed, final accepted version for American Mineralogist, published by the Mineralogical Society of America.
The published version is subject to change. Cite as Authors (Year) Title. American Mineralogist, in press.
DOI: https://doi.org/10.2138/am-2022-8756. http://www.minsocam.org/

INTRODUCTION

Most physical properties of solid materials are determined by how their electrons behave. Optical absorption behavior and color, for example, can be greatly affected by various electronic transition mechanisms. Intervalence charge transfer (IVCT) is one type. It can occur in crystals having cations with different formal valence states and in terms of minerals it has received considerable study over the last five decades or so. IVCT in most silicates takes place between the electronic *d* orbitals of transition metals residing in neighboring coordination polyhedra. Hetero- and homonuclear charge transfer can occur. A generalized example for the former, not considering the specifics of crystal chemistry, is $Fe^{2+} + Ti^{4+} \rightarrow Fe^{3+} + Ti^{3+}$ and for the latter $Fe^{2+} + Fe^{3+} \rightarrow Fe^{3+} + Fe^{2+}$. Both have been described for a number of different minerals[1]. The energies and intensities of IVCT electronic transitions depend on the crystal structure and composition of the minerals in question. They can be excited by radiation often corresponding to the visible region of the electromagnetic spectrum[2]. Optical absorption spectroscopy provides, therefore, an excellent method to investigate the process. Burns (1981, 1993) provides a very good and extensive treatment of the different electronic transitions that can occur in crystals as well as a discussion on optical absorption spectroscopy. He reviews the various known IVCT mechanisms known at the time for different minerals. Sherman (1987a, b) analyzed, in an early computational and theoretical treatment, $Fe^{2+} \rightarrow Fe^{3+}$ and $Fe^{2+} \rightarrow Ti^{4+}$ charge transfer transitions and thermally induced electron delocalization involving edge-sharing octahedral clusters.

The subject of IVCT in silicate garnet, general formula $\{X_3\}[Y_2](Z_3)O_{12}$, is not fully understood. This is because of the wide compositional range shown by different species, often extensive solid-solution behavior and the nature of the garnet crystal structure. Garnet can contain

[1] In early works (e.g., Burns 1981), the transitions were designated as $Fe^{2+} \rightarrow Ti^{4+}$ and $Fe^{2+} \rightarrow Fe^{3+}$.

[2] Thermally induced electron delocalization can also occur between adjacent Fe^{2+} and Fe^{3+} ions in some minerals (e.g., Sherman 1987).

various transition metals, which can occur in different formal oxidation states. Cations are located at three different crystallographically special positions having different coordination, namely triangular dodecahedral - {X}, octahedral - [Y] and tetrahedral - (Z). The M(etal)-O distances are different in the three polyhedra. Thus, chemical bonding behavior is variable throughout the crystal structure. What is known?

The Ca-Ti-bearing garnets are complex crystal chemically and initial research on IVCT concentrated on them. They can contain Fe at (Z) and [Y] and sometimes as well at {X}. Ti is located only at [Y] formally as a tetravalent cation, as discussed in Locock (2008). There are considerable spectroscopic (i.e., UV/Vis/NIR optical absorption and ^{57}Fe Mössbauer) and crystal-chemical results (e.g., Manning and Harris 1970; Dowty 1971; Moore and White 1971; Huggins et al. 1977a,b; Schwartz et al. 1980; Gangbao and Baolei 1986; Locock et al. 1995; Chakhmouradian and McCammon 2005). Heteronuclear $(Fe^{2+}) + [Ti^{4+}] \rightarrow (Fe^{3+}) + [Ti^{3+}]$ IVCT (Locock et al. 1995) and homonuclear $\{Fe^{2+}\} + (Fe^{3+}) \rightarrow \{Fe^{3+}\} + (Fe^{2+})$ IVCT (e.g., Schwartz et al. 1980) have been proposed. Both mechanisms involve iron occurring at (Z).

The aluminosilicate garnets, where X = Fe^{2+} (almandine), Mn^{2+} (spessartine), Ca (grossular), and Mg (pyrope) and where Y is nominally Al^{3+}, have also been investigated. They are simpler crystal chemically compared to the Ca-Ti-bearing group of garnets. They contain very little or no Fe at (Z) and the amount of formally Fe^{3+} and Ti^{4+} at [Y] is less. Platonov et al. (1991) and Langer et al. (1993) proposed in their UV/Vis spectroscopic studies IVCT of the type $\{Fe^{2+}\} + [Ti^{4+}] \rightarrow \{Fe^{3+}\} + [Ti^{3+}]$ for low titanium pyrope-grossular-almandine garnets occurring in mantle eclogites and other composition garnets found in various high-pressure metamorphic rocks, respectively. Taran et al. (2007) studied spectroscopically intermediate composition garnets, described as belonging to the system almandine-skiagite (i.e., $\{Fe^{2+}_3\}[Al^{3+}_2](Si_3)O_{12}$-$\{Fe^{2+}_3\}[Fe^{3+}_2](Si_3)O_{12}$) that crystallized in the upper mantle. They proposed IVCT of the type $\{Fe^{2+}\} + [Fe^{3+}] \rightarrow \{Fe^{3+}\} + [Fe^{2+}]$.

This is the peer-reviewed, final accepted version for American Mineralogist, published by the Mineralogical Society of America.
The published version is subject to change. Cite as Authors (Year) Title. American Mineralogist, in press.
DOI: https://doi.org/10.2138/am-2022-8756. http://www.minsocam.org/

Although lower pressure almandine-rich garnets, which are often found in various crustal rocks, could possibly show this latter electronic transition, it has not been reported. Moreover, it is not clear if $\{Fe^{2+}\} + [Fe^{3+}] \rightarrow \{Fe^{3+}\} + [Fe^{2+}]$ IVCT is restricted just to more iron-rich garnets. More study on different garnet species is needed in order to better understand the various possible electronic transitions and especially IVCT that can occur. We have measured the single-crystal optical absorption spectra primarily in the UV/Vis regions for a large number of garnet crystals (Geiger et al. Part I - in press; Taran et al. Part II - in press; Taran and Geiger unpublished). The former two studies focused largely on investigating the spin-forbidden electronic transitions relating to $\{Fe^{2+}\}$, $[Fe^{3+}]$ and $\{Mn^{2+}\}$.

In this work, we make further spectroscopic measurements on aluminosilicate garnet. Specifically, we concentrate our effort on understanding IVCT behavior in almandine-rich, spessartine-rich and grossular-rich crystals as well one intermediate composition almandine-pyrope garnet. Their spectra are described and analyzed. Finally, we make a review and an analysis of various possible IVCT mechanisms in both Ca-Ti-bearing and aluminosilicate garnets. The goal is to achieve a better and more complete understanding of the electronic transition behavior of an important rock-forming mineral group.

EXPERIMENTAL

Crystals used for study, UV/Vis/NIR spectroscopic measurements und spectral curve fitting

The garnets used for study are described in Table 1 and several are also listed in Geiger et al. (Part I - in press). The latter study describes many different garnet samples used in this broad ongoing investigation consisting of various spectroscopic research topics. The original crystal sizes vary between roughly 1-2 mm and 10 mm. A couple of garnets contain inclusions and they can also have various imperfections such as cracks and can sometimes show areas of alteration or reaction. This is the case for the two almandines studied here. Other crystals are largely clear and transparent

and can be described as almost gemmy like. The composition of grossular SGM-1 was measured using the procedure described in Geiger et al. (Part I - in press). Five measurement spots were made on the crystal.

It should be noted that careful preparation of crystal platelets of proper thickness and polish is important for quantitative spectroscopic measurements. Experience shows that platelets containing tiny inner defects and having surface imperfections can affect the nature of the spectral background. This can complicate spectra fitting and determinations of the model band properties. In order to make good measurements in the UV/Vis/NIR regions on small crystals or on crystal with various imperfections, a microscope spectrometer is necessary. The device used in this investigation in Kyiv is described in Part I. Measurements were made at room temperature.

The measured UV/Vis spectra were curve-fit using Jandel Scientific Peakfit 4.11 software in order to obtain quantitative information on different electronic absorption features, which are often overlapped in the case of Fe-containing garnet spectra. Fitted IVCT and spin-forbidden bands are assumed to be Gaussian in shape, whereas the ligand-metal charge-transfer absorption edge is modeled using a combination of Gaussian and Lorentzian functions. The assumptions involved in fitting garnet spectra and the inherent uncertainties are discussed in Taran et al. (Part II - in press).

RESULTS

Garnet compositions and UV/Vis spectra of the different garnet species

The garnet compositions in oxide weight percent and their crystal-chemical formulae in terms of end-member garnet components are found in Table 2a and 2b, respectively. Table 3 gives the crystal-chemical formulas of various garnets that have been studied spectroscopically and the results published in the literature. They are discussed below. Figures 1 to 5 show the measured single-crystal UV/Vis/NIR spectra and their fits for the different garnet samples.

This is the peer-reviewed, final accepted version for American Mineralogist, published by the Mineralogical Society of America.
The published version is subject to change. Cite as Authors (Year) Title. American Mineralogist, in press.
DOI: https://doi.org/10.2138/am-2022-8756. http://www.minsocam.org/

Nearly end-member almandine. Figure 1a shows the measured UV/Vis/NIR optical absorption spectrum of a nearly end-member almandine, sample FR-3 (Woodland et al. 1995) and its fit. It has composition $\{Fe^{2+}_{2.83}Mg_{0.07}Ca_{0.09}\}[Al_{1.92}Fe^{3+}_{0.08}](Si_{2.99})O_{12}$. Intense absorption occurs in the visible region with a maximum centered at roughly 21000 cm^{-1}. Several weak and relatively narrow absorption features that are superimposed on the broad absorption envelope can be observed in the spectrum. A relatively strong narrow band is also observed in the UV region at about 27000 cm^{-1}. It sits upon the low-energy oxygen-metal charge-transfer edge that is part of an extremely intense absorption feature whose peak maximum is located much further into the UV region. This oxygen-metal CT edge is present in all of the following spectra with varying degrees of absorption as a function of wavenumber (see also Taran et al. Part II - in press).

Figure 1b shows the spectrum of a second almandine-rich crystal, sample JF-1 (Aparicio et al. 2012), of composition $\{Fe^{2+}_{2.81}Mg_{0.11}Mn^{2+}_{0.01}Ca_{0.05}\}[Al_{1.97}Fe^{3+}_{0.04}](Si_{2.99})O_{12}$. Its UV/Vis/NIR spectrum shows absorption over much of the visible region with a maximum centered once again at roughly 21000 cm^{-1}, but it is less intense than that observed in the spectrum of FR-3. There are a number of other narrow and weak absorption features that are better resolved compared to those in the spectrum of FR-3 .

Intermediate composition almandine-pyrope garnet. Figure 2 shows the spectrum of an intermediate almandine-pyrope garnet, sample GTF 90-33. Its composition is $\{Fe^{2+}_{1.39}Mg_{1.33}Ca_{0.20}Mn^{2+}_{0.06}\}[Al_{1.92}Fe^{3+}_{0.09}Ti^{4+}_{0.01}](Si_{2.97}Al_{0.03})O_{12}$ (see also Table 3), as calculated using the data in Taran et al. (2007) and using the formulation of Locock (2008). It was first studied spectroscopically by Taran et al. (2007). The original crystal platelet from this investigation was repolished and its spectrum was measured once again for this work. Its UV/Vis/NIR spectrum is broadly similar to that of almandine JF-1 in terms of band behavior but the overall absorption is slightly less.

This is the peer-reviewed, final accepted version for American Mineralogist, published by the Mineralogical Society of America.
The published version is subject to change. Cite as Authors (Year) Title. American Mineralogist, in press.
DOI: https://doi.org/10.2138/am-2022-8756. http://www.minsocam.org/

179

180 **Spessartine-rich garnet.** Two different spessartine-rich garnets were investigated, sample 316306
181 (370928271669) of composition $\{Mn^{2+}_{2.30}Fe^{2+}_{0.47}Mg_{0.15}Ca_{0.09}\}[Al_{1.97}Fe^{3+}_{0.02}Ti^{4+}_{0.01}](Si_{3.00})O_{12}$ and
182 sample 200924241653 of composition $\{Mn^{2+}_{2.09}Fe^{2+}_{0.86}Ca_{0.04}\}[Al_{1.99}Ti^{4+}_{0.01}](Si_{3.00})O_{12}$. Figures 3a
183 and b show their respective spectra and both are different in appearance compared to almandine-
184 rich garnets. For example, several narrow absorption features (i.e., spin forbidden bands of $\{Mn^{2+}\}$
185 (Taran et al. Part II - in press) are observed at higher energies of the visible region. Similar to the
186 case of the almandine spectra, there is also broad absorption between about 15000 and 25000 cm^{-1}
187 with a maximum intensity roughly around 21000 cm^{-1}. The amount of absorption in the visible
188 region is less compared to the spectra of almandine garnets.

189

190 **Nearly end-member grossular.** Two different grossular-rich garnets were investigated. Sample
191 SGM-1 has composition $\{Ca_{2.79}Fe^{2+}_{0.19}Mg_{0.02}Mn^{2+}_{0.01}\}[Al_{1.94}Fe^{3+}_{0.04}Ti^{4+}_{0.02}](Si_{2.99}Al_{0.01})O_{12}$. Its
192 spectrum shows absorption, which starts with increasing energy at about 15000 cm^{-1}, that extends
193 into the UV region with generally increasing absorption (Fig. 4a). Three weak absorption features
194 can also be observed, the most prominent of which is located at about 27000 cm^{-1} (Fig. 4a).

195 The second grossular, GR 10074, has a nearly end-member composition of
196 $\{Ca_{2.91}Fe^{2+}_{0.07}\}[Al_{1.96}Fe^{3+}_{0.04}](Si_{3.00})O_{12}$. Its spectrum (Fig. 4b) is broadly similar to that of SGM-1,
197 but it has even less optical absorption. Several weak features are observed with the most intense,
198 once again, located at about 27000 cm^{-1}. They are superimposed on a much broader absorption that
199 occurs over much of the visible region.

200

201 **DISCUSION**

202 **UV/Vis spectra and IVCT in aluminosilicate garnet**

Geiger et al. (Part I - in press) and Taran et al. (Part II - in press) measured the single-crystal UV/Vis/NIR spectra of a number of garnets with compositions corresponding to the almandine-pyrope and almandine-spessartine binaries (see Figs. 2 and 4 of the former work). The spectra of the almandine-pyrope garnets, for example, display a number of relatively weak and narrow spin-forbidden bands that can be assigned to $\{Fe^{2+}\}$ and $[Fe^{3+}]$. Most of these spectra are, however, notably different from those of the almandine-rich and intermediate almandine-pyrope garnets studied in this work in one key respect. The difference lies in the presence or absence of elevated absorption over much of the visible region beyond that given by the various overlapping and narrow spin-forbidden bands. We focus much of our analysis on the nature of this elevated absorption in the spectra of the garnets investigated herein.

Nearly end-member almandine. Nearly end-member almandine, FR-3, is one of the most almandine-rich natural garnets described to date (Woodland et al. 1995) having 93.5% of an almandine component (Table 2b). Formal $[Fe^{3+}]$ can be calculated from the microprobe analysis and it can be assigned to andradite (2.93 mol %) and skiagite (0.77 mol %) components following the formulation of Locock (2008). The ^{57}Fe Mössbauer spectra of several garnets from this locality show a small Fe^{3+} doublet, placing the ferric iron at the octahedral site, and an atomic $Fe^{3+}/\sum Fe$ ratio of 3-4 % is obtained (Woodland et al. 1995). The color of a thin crystal platelet is firebrick red.

The UV/Vis/NIR spectrum and its fit are shown in Figure 1a and the properties of the different fitted bands are given in Supplementary Table 1. This exercise gives a very broad intense band (i.e., FWHM ≈ 5794 cm^{-1}) centered at 21389 cm^{-1} that dominates the higher energy visible region. Because this nearly end-member almandine does not contain any transition metal in significant concentrations other than Fe and considering the analysis of Taran et al. (2007), we assign this intense absorption feature to a $\{Fe^{2+}\} + [Fe^{3+}] \rightarrow \{Fe^{3+}\} + [Fe^{2+}]$ IVCT transition.

Weaker absorption features can also be fit to the spectrum and are given in Supplementary Table1. They are assigned to electronic spin-forbidden transitions of $\{Fe^{2+}\}$ and $[Fe^{3+}]$ and are labeled following Moore and White (1972) and Taran et al. (Part II - in press). In terms of the latter type, the band labeled l at 23030 cm^{-1} and the band m at 23476 cm^{-1} can be assigned to the crystal-field independent transitions $^6A_1 \rightarrow {}^4A_1, {}^4E\ ({}^4G)$. Band r at 27030 cm^{-1} is assigned to a higher energy $^6A_1 \rightarrow {}^4E\ ({}^4D)$ $[Fe^{3+}]$ crystal-field independent transition. Such transitions typically manifest themselves as relatively sharp and distinct absorption features in the case of ions with the d^5 electronic configuration. A band at 26480 cm^{-1}, marked as "??", which has no clear expression in the experimental spectrum, is obtained in the deconvolution. It may be related to the $^6A_{1g} \rightarrow {}^4T_{2g}\ ({}^4D)$ transition of $[Fe^{3+}]$ (Taran et al. 2007; Taran et al. Part II - in press). The remaining weak bands are assigned to various $\{Fe^{2+}\}$ spin-forbidden transitions.

Figure 1b shows the spectrum of a second almandine-rich crystal, JF-1, and its curve fit. The parameters for the latter are summarized in Supplementary Table 2. The most prominent absorption feature from the fit of the spectrum is centered at 21638 cm^{-1} and it has a FWHM = 6434 cm^{-1}. It is assigned, as in the case of almandine FR-3, to a $\{Fe^{2+}\} + [Fe^{3+}] \rightarrow \{Fe^{3+}\} + [Fe^{2+}]$ IVCT transition. The less intense and more narrow features are again spin-forbidden transitions of $\{Fe^{2+}\}$ and $[Fe^{3+}]$. They are more distinct in the experimental spectrum compared to the bands in the spectrum of almandine FR-3 (cf. Fig. 1a) because the IVCT is weaker. The overall absorption (i.e., linear absorption coefficient) shown by garnet JF-1 in the UV/Vis region is considerably less compared to that observed in the spectrum of almandine FR-3. This is case although both have very similar percentages of an almandine component, namely 93.6% and 93.5%, respectively. It is also of note that the spin-forbidden Fe^{3+} band r at 27055 cm^{-1} has about one quarter the intensity of band r in the spectrum FR-3 (see Taran et al. Part II - in press - for a discussion of the intensity behavior of this electronic transition in garnet). Thus, almandine JF-1 has less $[Fe^{3+}]$ than FR-3, as also shown by its ^{57}Fe Mössbauer spectrum (see Aparicio et al. 2012). The product of the formal

253 divalent and trivalent atomic iron concentrations, $\{Fe^{2+}\} \times [Fe^{3+}]$, should describe the number of
254 local Fe^{2+}-Fe^{3+} pairs. This product is less for JF-1 compared to that for almandine FR-3 and,
255 therefore, the IVCT absorption in the spectrum of the former is less than in the latter.
256
257 **Intermediate almandine-pyrope solid solution.** Garnet, GTF 90-33, is an intermediate almandine-
258 pyrope crystal of roughly 50-50 composition (Table 3). Its UV/Vis/NIR spectrum is shown in Fig. 2
259 and the fitted band parameters, obtained from its deconvolution, are summarized in Supplementary
260 Table 3. The intensities of the various Fe^{2+} and Fe^{3+} spin-forbidden bands and the broad IVCT band
261 are approximately similar to those in the spectrum of JF-1. Geiger et al. (Part I - in press) discuss
262 wavenumber behavior for the different energy Fe^{2+} and Fe^{3+} spin-forbidden bands along the
263 almandine-pyrope binary.
264
265 **Spessartine-rich garnet.** End-member spessartine has the crystal-chemical formula
266 $\{Mn^{2+}_{3.00}\}[Al_{2.00}](Si_{3.00})O_{12}$. Crystals close to this composition occur in nature and they are orange
267 in color (Laurs and Knox 2001). Most natural spessartines show varying amounts of other garnet
268 components, the primary one often being almandine. These crystals take on red and/or darker
269 colorations as in samples 316306 (370928271669) and 200924241653. The former sample was
270 obtained as a faceted stone and is "classic" red and the latter was obtained as a cabochon and it is
271 more reddish orange in coloration. Both garnets are solid solutions and they have about 77 and 70
272 mol % of a $Mn^{2+}_3Al_2Si_3O_{12}$ component and 15 and 29 mol % of a $Fe^{2+}_3Al_2Si_3O_{12}$ component,
273 respectively (Table 2b). Based on the microprobe results, spessartine 316306 contains formally Fe^{3+}
274 and a little Fe^{2+} in octahedral coordination (i.e., held as andradite and morimotoite components,
275 respectively).
276 The UV/Vis/NIR spectra of both spessartines and their fits show four, possibly five, narrow
277 Mn^{2+} spin-forbidden bands (p, o, n, n', and unlabeled) located between 22500 and 24500 cm^{-1} (Fig.

278 3a and 3b and Supplementary Tables 4 and 5). They are characteristic for spessartine-rich garnet
279 (Taran et al. Part II - in press). Both spectra also show with increasing energy absorption starting at
280 about 15000 cm^{-1} that increases with increasing wavenumber. A very broad band can be fit to both
281 spectra having a maximum intensity at ~20547 cm^{-1} and ~20880 cm^{-1} for 316306 (370928271669)
282 and 200924241653, respectively (Supplementary Tables 4 and 5). This band in the spectrum of the
283 latter spessartine is about two times more intense than in the former. We think this absorption
284 feature in both spectra is due to $\{Fe^{2+}\} + [Fe^{3+}] \rightarrow \{Fe^{3+}\} + [Fe^{2+}]$ IVCT. This electronic transition
285 has not been recognized pr proposed before for spessartine to the best of our knowledge. The
286 spectra of other spessartine-rich garnets, for example those investigated by Geiger et al. (Part I - in
287 press) and Taran et al. (Part II - in press), do not show this absorption feature or it is too weak to be
288 observed and fit. We do have, though, other unpublished spessartine spectra where it is present.
289
290 **Nearly end-member grossular.** End-member grossular, $\{Ca^{2+}_{3.00}\}[Al_{2.00}](Si_{3.00})O_{12}$, is colorless. It
291 shows no absorption in the visible region. Colorless crystals can be found in nature, but the great
292 majority of grossulars show color and they can be very different. They can be green, yellow, amber,
293 brownish, pink, orange red, and raspberry red, for example.
294 The grossular-rich crystal SGM-1 was obtained as a faceted stone and its color is roughly
295 brownish orange red. It has about 90 mol % of a grossular component. Small amounts of andradite,
296 schorlomite and morimotoite are calculated form the microprobe results (Table 2b). Its UV/Vis
297 spectrum appears relatively simple in terms of absorption behavior and the number bands (Fig. 4a).
298 The results for the curve fit of the spectrum are given in Supplementary Table 6. They reveal a
299 broad band centered at ~22700 cm^{-1}. It lies at higher energies compared to the IVCT bands of the
300 other studied garnets and it is noticeably broader with a FWHM of about 8700 cm^{-1}. The absorption
301 and this band feature are difficult to interpret fully and precisely. This grossular contains about 0.02
302 $[Ti^{4+}]$, 0.04 $[Fe^{3+}]$ and 0.01 $[Fe^{2+}]$ formal atoms pfu. Thus, it is possible that both $\{Fe^{2+}\} + [Ti^{4+}] \rightarrow$

303 $\{Fe^{3+}\} + [Ti^{3+}]$ and $\{Fe^{2+}\} + [Fe^{3+}] \rightarrow \{Fe^{3+}\} + [Fe^{2+}]$ IVCT may be occurring in this garnet (see
304 discussion below). The weaker, narrower bands at 23119 (m), 26235 ("??") and 26984 cm^{-1} (r)
305 likely represent $[Fe^{3+}]$ spin-forbidden transitions.

306 The second crystal that was studied, GR 10074, is quite close to end-member grossular in
307 composition containing about 97 mol % $Ca_3Al_2Si_3O_{12}$ (Table 2b). The amounts of the calculated
308 almandine and andradite components are 2.4% and 0.4%, respectively. The sample was investigated
309 by Palke et al. (2015) and they measured its ^{27}Al and ^{29}Si MAS NMR spectra, concentrating on the
310 paramagnetically shifted resonances. Its ^{57}Fe Mössbauer spectrum was recorded as well and is
311 shown in Fig. 5. The weaker quadrupole doublet is assigned to Fe^{3+} at the octahedral site and the
312 stronger one to Fe^{2+} at the dodecahedral site. The platelet prepared from this crystal has a
313 considerable thickness of 3.5 mm and its color is brownish red. The optical absorption spectrum
314 shows very little absorption across the Vis region compared to the other studied garnets (Fig. 4b).
315 The curve fit to the spectrum gives a broad band (FWHM ≈ 5904 cm^{-1}) centered at ~21190 cm^{-1},
316 but both these values have uncertainty due the low overall absorption (see Supplementary Table 7).
317 A number of more narrow, weak absorption features between 23000 and 24500 cm^{-1} can be fit as
318 well and they are spin-forbidden Mn^{2+} bands. Those bands or features at lower energies can be
319 assigned to Fe^{2+}. The highest wavenumber bands at 25942 and 26966 cm^{-1} are assigned to the $[Fe^{3+}]$
320 spin-forbidden transitions $^6A_{2g} \rightarrow {}^4T_{2g}$ (^4D) and $^6A_{2g} \rightarrow {}^4E_g$ (^4D). We think that the broad band in
321 the spectrum of this iron-poor grossular results from $\{Fe^{2+}\} + [Fe^{3+}] \rightarrow \{Fe^{3+}\} + [Fe^{2+}]$ IVCT. This
322 electronic transition has not been reported for grossular before to the best of our knowledge.
323
324 **IVCT transition behavior and energy and crystal chemistry and Fe structural state**
325 The spectroscopic results, herein, show that $\{Fe^{2+}\} + [Fe^{3+}] \rightarrow \{Fe^{3+}\} + [Fe^{2+}]$ IVCT
326 appears to occur in different garnet species and even those not rich in iron. It is, thus, a general

electronic transition mechanism. Sherman (1987a), who focused his theoretical analysis on Fe^{2+} and Fe^{3+} in model polyhedral clusters, used the term asymmetric IVCT to describe electronic exchange between Fe atoms occurring in neighboring coordination sites. It takes place between Fe^{2+} and Fe^{3+} through an overlap of their *d* orbitals. It would appear that the oxygen anions at the corners of the respective coordination polyhedra are not directly involved in the IVCT.

The exact distances between iron atoms in a solid-solution garnet crystal cannot be measured quantitatively via diffraction, because the precise nature of local structural relaxation is not known. The $\{Fe^{2+}\}$-$[Al^{3+}]$ distance in end-member almandine (Armbruster et al. 1992) is 3.2213 Å, the $\{Ca^{2+}\}$-$[Al^{3+}]$ distance in end-member grossular is 3.3116 Å (Geiger and Armbruster 1997) and the $\{Ca^{2+}\}$-$[Fe^{3+}]$ distance in end-member andradite is 3.3628 Å (Armbruster and Geiger 1993). Because of the relatively long Fe-Fe distances, which should be roughly 3.4 Å, and the different nature of the Fe potentials. $\{Fe^{2+}\} + [Fe^{3+}] \rightarrow \{Fe^{3+}\} + [Fe^{2+}]$ IVCT in garnet occurs at relatively high energies compared to various $Fe^{2+} + Fe^{3+} \rightarrow Fe^{3+} + Fe^{2+}$ IVCT measured in the spectra of other silicates[3]. Here, the transition energies lie between about 9700 and 19000 cm^{-1} (Burns 1981, 1993). In most silicates and oxides studied to date, IVCT typically occurs between Fe atoms in edge-sharing or, more seldom, face-sharing octahedra. Figure 6 shows and compares the various IVCT bands fitted to the different garnet spectra. It can be seen that the band maximum for grossular SGM-1 is at higher energies compared to that in the spectra of the other garnets. It can be argued, therefore, once again, that $\{Fe^{2+}\} + [Ti^{4+}] \rightarrow \{Fe^{3+}\} + [Ti^{3+}]$ IVCT is also occurring in this garnet as well (see discussion below).

The crystal-chemical formulas of the studied garnets were calculated using the formulation of Locock (2008). His model indicates for the different garnets that Fe^{3+} is held mostly as a $Ca_3Fe^{3+}{}_2Si_3O_{12}$ component and a minor skiagite component, $\{Fe^{2+}{}_3\}[Fe^{3+}{}_2](Si_3)O_{12}$, is calculated as

[3] However, as best we know, there is no theoretical work that shows that the energy of an electronic IVCT transition depends on the donor-acceptor distance of a metal pair (e.g., Wong et al. 1979, Cox 1980, Girerd 1983, Sherman 1987a, b).

well for almandine FR-3 (Table 2b - a very small amount of a $\{Ca_3\}[Ti^{4+}Fe^{2+}_2](SiAl_2)O_{12}$ component is obtained for spessartine 316306). A $Ca_3Fe^{3+}_2Si_3O_{12}$ component is also calculated for the "almandine-skiagite" garnets (Table 3) investigated by Taran et al. (2007). It goes without saying that such a crystal-chemical calculation, based solely on analytical microprobe data, is model dependent. Assumptions are made in allocating the atoms to the different end-member garnet components in an assumed calculation sequence. Such an analytically based scheme cannot be used, *a priori*, to determine the actual local arrangements of atoms in the various garnet crystal structures. To determine them further research will be required. Consider now the crystal-chemical behavior of the Fe atoms and their possible structural state.

The $\{Fe^{2+}\} + [Fe^{3+}] \rightarrow \{Fe^{3+}\} + [Fe^{2+}]$ IVCT occurs within the triangular dodecahedral-octahedral garnet sublattice. Each octahedron in the garnet structure shares six of its twelve edges with neighboring triangular dodecahedra and each triangular dodecahedron shares four edges with surrounding octahedra (see Figs. 1b and 1c in Geiger et al. Part I - in press). The precise possible local Fe atomic configuration and their number that are involved in the electronic transition cannot be established. In other words, it is not possible to determine from the UV/Vis spectra how many $\{Fe^{2+}\}$ cations surround a central $[Fe^{3+}]$ cation or how many $[Fe^{3+}]$ cations surround a central $\{Fe^{2+}\}$ cation.

The spectra do allow, though, a simple first-order crystal chemical analysis. First, it is notable that IVCT occurs in a grossular crystal (i.e., GR 10074) with only 2.4 % of a $Fe^{2+}_3Al_2Si_3O_{12}$ and 0.4 % of a $Ca_3Fe^{3+}_2Si_3O_{12}$ component. There are two possible interpretations. This first is, if one assumes a statistically random distribution of formally charged $\{Fe^{2+}\}$ and $[Fe^{3+}]$ cations in the grossular structure, that the IVCT is so intense that the existence of just very few local Fe^{2+}-Fe^{3+} pairs in the grossular can give rise to measurable absorption. In this regard, it should be noted that the extinction coefficient values (e.g., l/mol·cm) for $Fe^{2+} \rightarrow Fe^{3+}$ IVCT in crystals lie between about 10^2 to 10^3 compared to about 10^{-3} to 1 for the values of spin-forbidden Fe^{3+} bands (Burns 1993 -

Table 3.6). The second possibility to account for IVCT is that local Fe^{2+}-Fe^{3+} pairing or clustering (i.e., short range ordering) occurs in the grossular. The sizes of any such possible clusters cannot be determined. Geiger et al. (2019) suggested, based on an analysis of the low-temperature magnetic transition heat-capacity behavior of grossular-andradite solid solutions, that superparamagnetism (i.e., clustering of Fe^{3+} cations) could possibly occur in grossular-rich compositions. On the other hand, Palke et al. (2015) were not able to detect in their NMR investigation any overt short-range Fe^{3+} ordering in grossular GR 10074.

In this latter regard, it is noted that the intensity of the IVCT band is similar for almandine JF-1, the almandine-pyrope garnet GTF 90-33 and spessartine 200924241653 (Fig. 6), although they have very different Fe concentrations. They are 42.53, 23.42 and 12.50 in terms of wt.% FeO, respectively. Based on similarity of IVCT band intensities, the number of local Fe^{2+}-Fe^{3+} pairs or clusters should be similar in the three crystals. This could possibly indicate that some or more Fe short-range clustering could be present in the Fe-poorer garnets.

IVCT and color

$\{Fe^{2+}\} + [Fe^{3+}] \rightarrow \{Fe^{3+}\} + [Fe^{2+}]$ IVCT can greatly affect the color of garnet. The absorption maximum of the corresponding absorption band is centered in the blue region of the visible spectrum and its flanks extend at higher energies into the ultra-violet and at lower energies into the orange region. The effect is best and most simply illustrated in the case of grossular, because $Ca_3Al_2Si_3O_{12}$ is colorless. The IVCT band is the strongest absorption feature in the spectra of the two studied grossulars (Fig. 4) and is, thus, the key electronic transition mechanism in determining color. Light absorption is weakest in the red region and this explains the observed crystal colorations. The high wavenumber spin-forbidden bands, such as those related to Mn^{2+} and Fe^{3+}, also play a role in determining color, as does the low-energy edge of the oxygen $\rightarrow$ metal charge transfer band(s).

400

401 **Geological conditions of formation and crystallization**

402 The geologic environments and crystallization conditions for several of the garnets under
403 study are considered as well as those investigated by Taran et al. (2007). This is done in order to
404 determine if there are certain common formation conditions of the studied garnets that could give
405 rise to IVCT.

406

407 **Almandine**. Garnet FR-3 is from an ironstone metamorphosed at 630 ± 60 °C and 5 ± 2 kbar
408 (Woodland et al. 1995). These rocks are free of quartz and contain nearly end-member fayalite. The
409 f_{O_2} during crystallization was relatively reduced being below the FMQ (i.e., fayalite-magnetite-
410 quartz) buffer.

411 The geologic history of the area from which almandine JF-1 was taken is discussed by
412 Souček (1978). While the exact locality and rock unit is not known, the region consists of volcanic
413 and sedimentary units that were regionally metamorphosed in two events. The younger event
414 occurred at medium pressure (5.5 kb) and over various temperatures.

415 The intermediate composition almandine-pyrope garnet, GTF-33, comes from Cortlandt,
416 New York, and the rocks there were investigated by Barker (1964) and Dorfler et al. (2015). The
417 Cortlandt Complex consists largely of mafic intrusive rocks in which xenoliths of pelitic schists,
418 some containing garnet, are found. The metamorphic grade of the xenoliths was described as
419 belonging to the hornfels facies in the former study, thus being relatively low pressure in origin.
420 The latter study makes a more quantitative analysis of the metamorphic history and *P-T-X*
421 conditions. Pressure was considered to be less than 1 kb and garnet was present over range of
422 temperatures during a rapid heating event that reached a maximum temperature of about 1200 °C.

In terms of the garnets studied by Taran et al. (2007), several of the Fe-rich crystals came from mafic granulites that crystallized at pressures corresponding to the upper mantle (Spetsius and Serenko 1990).

Grossular. Nearly end-member composition crystals such as GR 10074 can be found in rodingites associated with serpentinites as at Asbestos, Quebec, Canada. The geological setting and polymetamorphic history of the rocks at Asbestos are complex and evolved. Normand and Williams-Jones (2007) describe three metamorphic events in the formation of these rocks and they analyzed the *P-T* conditions. All events were relatively low grade in nature (e.g., 290 to 360 °C and 2.5 to 4.5 kb for the first, 325 to 400 °C and less than 3 kb for the second, and a third, even lower-grade event occurring late in the geologic history).

Based on this first, simple analysis involving a limited number of garnet samples there does not appear to be any specific *P-T-X* crystallization conditions that give rise to common crystal-chemical properties that lead to IVCT.

A review and analysis of various possible IVCT mechanisms in the silicate garnet group

Burns (1993) reviewed various IVCT mechanisms for a number of different minerals. Since his review, several spectroscopic investigations on garnet have been published and new IVCT mechanisms have been proposed. Multiple mechanisms can arise for a couple of reasons. First, the garnet group as a whole can contain various transition metals and in different oxidation states. Second, the garnet crystal structure is cubic, *Ia*-3*d*, and it has three different cation sites with different oxygen coordination polyhedra. There exists a three-dimensional network of interconnected coordination polyhedra and three types of polyhedral sublattices exist.

Table 4 summarizes the state of the field in terms of the various proposed IVCT mechanisms in silicate garnet. The Ca-Ti-bearing and aluminosilicate garnets are separated in this table inasmuch as their chemistries are different and, although they are isostructural, they show different structural behavior (Novak and Gibbs 1971). The aluminosilicate garnets often contain $\{Fe^{2+}\}$ and often as a major element, whereas some Ca-Ti silicate garnets appear to be free of this ferrous iron. The Ca-Ti garnets can, in turn, contain significant amounts of $[Fe^{2+}]$ and (Fe^{3+}), whereas the aluminosilicate species do not have $[Fe^{2+}]$ and $(Fe^{2,3+})$ or they are present in very minor concentrations. The aluminosilicate garnets, excepting grossular, contain minor amounts of Fe^{3+} and Ti^{4+} at [Y]. In Ca-Ti garnets, their concentrations are considerably higher.

Several pyrope-grossular-almandine garnets from mantle eclogites were studied by UV/Vis optical absorption spectroscopy (Platonov et al. 1991). The garnets contained between 0.009 and 0.031 $[Ti^{4+}]$ pfu. These researchers observed a broad absorption feature (FWHM of about 7000 cm^{-1}) whose maximum was estimated to lie between 23500 to 23700 cm^{-1}. They assigned this absorption feature to heteronuclear IVCT of the type $\{Fe^{2+}\} + [Ti^{4+}] \rightarrow \{Fe^{3+}\} + [Ti^{3+}]$ based on a good linear correlation between the band intensity and the mole fraction product $X_{Fe^{2+}} \cdot X_{Ti^{4+}}$ in their garnets. We reproduced one of their spectra (sample N25) and fitted it in order to analyze it more fully (Supplementary Fig. 1a). The IVCT band has a peak maximum at 23475 cm^{-1} and it is, thus, roughly 1500-2500 cm^{-1} higher in energy than homonuclear $\{Fe^{2+}\} + [Fe^{3+}] \rightarrow \{Fe^{3+}\} + [Fe^{2+}]$ IVCT in garnet (Taran et al 2007; this work). The FWHM of the band is 8255 cm^{-1}, which is quite large. According to the model cluster-type calculations of edge-sharing octahedra Sherman (1987a,b), Fe^{2+}-Ti^{4+} charge transfer energies are higher than those associated with Fe^{2+}-Fe^{3+}. The situation in garnet is consistent with this result. We considered, furthermore, the possibility that this absorption feature could consist of two bands representing both types of IVCTs. Thus, a fit with two bands was made to the spectrum of garnet N25 of Platonov et al. (1991). The result is shown in

Supplementary Fig. 1. Their band energies are 24053 and 20474 cm^{-1} and they have FWHM values of 4645 and 5358 cm^{-1}, respectively,

In a second spectroscopic investigation, Langer et al. (1993) investigated different aluminosilicate garnets from diamondiferous high-pressure metamorphic rocks. We analyze the results from one of their crystals (sample 257). To start, we calculated its crystal-chemical formula (Table 2). This garnet contains nearly 50% $\{Fe^{2+}{}_3\}[Al_2](Si_3)O_{12}$ and 1.69% $\{Ca_3\}[Ti^{4+}Fe^{2+}](Si_3)O_{12}$ and 0.82% $\{Ca_3\}[Fe^{3+}](Si_3)O_{12}$. The number of octahedrally coordinated Ti^{4+} and Fe^{3+} atoms is very similar, that is 0.017 and 0.016, respectively, and slight amounts of Fe^{2+}, also octahedrally coordinated, are calculated as well. Langer et al. (1993) observed in their UV/Vis spectrum of sample 257 a strong absorption feature, whose energy they estimated to be 21500 cm^{-1}. They assigned it, as in the study of Platonov et al (1991), to $\{Fe^{2+}\} + [Ti^{4+}] \rightarrow \{Fe^{3+}\} + [Ti^{3+}]$ IVCT. We reproduced this spectrum and fit it. We obtain an intensity maximum of 22271 cm^{-1} for the band describing the strong absorption feature (Supplementary Fig. 2). It is difficult for us to assign it with certainty. Based on the results of this work, it could be assigned to $\{Fe^{2+}\} + [Fe^{3+}] \rightarrow \{Fe^{3+}\} + [Fe^{2+}]$ IVCT (see Fig. 6). The nature of the problem is difficult, because IVCT bands are very broad. If both $\{Fe^{2+}\} + [Ti^{4+}] \rightarrow \{Fe^{3+}\} + [Ti^{3+}]$ and $\{Fe^{2+}\} + [Fe^{3+}] \rightarrow \{Fe^{3+}\} + [Fe^{2+}]$ IVCT are present in garnet, their respective absorption bands will overlap. It is possible that two different IVCT mechanisms may be operating in this garnet and others as well as such as grossular SGM-1. At any rate and to summarize, based on the results of Platonov et al. (1991), Langer et al. (1993) and Taran et al. (2007) both types of IVCT can occur in aluminosilicate garnet (Table 4).

Consider now the Ca-Ti silicate group of garnets and the spectroscopic work that has been done on them. Here, additional IVCT mechanisms have been proposed (Table 4). In early studies, IVCT of the type $\{Fe^{2+}\} + (Fe^{3+}) \rightarrow \{Fe^{3+}\} + (Fe^{2+})$ was suggested as a possibility (Moore and White 1972; Schwartz et al. 1980). However, the associated band at of 5280 cm^{-1} appears to be too narrow to represent charge transfer (Locock et al. 1995) and, moreover, its energy is much lower

compared to those of various other IVCT bands observed in many different minerals (Burns 1993). For both reasons, this interpretation is questionable.

Locock et al. (1995) argued for another IVCT mechanism in their crystal-chemical and multi-spectroscopic study of schorlomite of composition $\{Ca_{2.866}Mg_{0.080}Na_{0.038}Mn_{0.019}\}_{\Sigma 3.003}[Ti^{4+}_{1.058}Fe^{3+}_{0.6.31}Al_{0.137}Fe^{2+}_{0.057}Mg_{0.055}Zr_{0.039}V^{3+}_{0.014}Mn_{0.013}]_{\Sigma 2.004}(Si_{2.348}Fe^{3+}_{0.339}Fe^{2+}_{0.331}[4H]_{0.005})_{\Sigma 3.003}O_{12}$. They argued that an intense absorption feature at about 20000 cm^{-1} in their UV/Vis spectrum was caused by $[Ti^{4+}] + (Fe^{2+}) \rightarrow [Ti^{3+}] + (Fe^{3+})$ IVCT. They discuss at length the reasons for this assignment, which is somewhat unusual. This is because electron delocalization of a superexchange type must occur through the intervening oxygen atoms of neighboring corner-shared Fe-centered tetrahedra and Ti-centered octahedra. In this regard, it is worth noting that magnetic superexchange interactions occur at very low temperatures below 15 K in iron-bearing silicate garnets. Here, the *d*-electron spin interactions of Fe^{2+} or Fe^{3+} are mediated through the intervening oxygen *p* orbitals (Geiger et al. 2019). It should also be noted that superexchange-like IVCT has been observed in various synthetic molecular crystals containing different metals (e.g., Holwerda et al. 1998) and including iron (Suzuki et al. 1998). This type of IVCT has not been documented in other silicates as best we know.

IMPLICATIONS

IVCT of the type $\{Fe^{2+}\} + [Fe^{3+}] \rightarrow \{Fe^{3+}\} + [Fe^{2+}]$ can occur in different aluminosilicate garnet species and over a range of solid-solution compositions. It is, therefore, a general electronic transition. It is not necessarily restricted to specific garnet species or compositions and it does not require a narrow range of *P-T-X* conditions of crystallization, for example, high pressures. How extensive it really is and for which of the many garnet species (Grew et al. 2013) remains to be determined. Many published UV/Vis/NIR spectra of garnet, as well as a large number of our own (Geiger et al. Part I - in press; Taran et al. Part II - in press, Taran and Geiger unpublished), do not

This is the peer-reviewed, final accepted version for American Mineralogist, published by the Mineralogical Society of America.
The published version is subject to change. Cite as Authors (Year) Title. American Mineralogist, in press.
DOI: https://doi.org/10.2138/am-2022-8756. http://www.minsocam.org/

show any IVCT band, although weak, indiscernible absorption could be hidden in spectra that are dominated by a number of overlapping spin-forbidden transitions. On the other hand, we note that absorption due to IVCT can be observed in the spectra of some published (or online) spectra of garnet. We also have unpublished spectroscopic results showing its presence. Why $\{Fe^{2+}\} + [Fe^{3+}] \rightarrow \{Fe^{3+}\} + [Fe^{2+}]$ IVCT is observed in the spectra of some garnets but not in other garnet crystals of similar composition remains to be determined.

Recent research on transition-metal-bearing silicate garnets is starting to reveal more about their electronic and magnetic behavior. The local physical mechanisms behind them are often subtle and complex in nature. Much further research is needed to determine how they affect macroscopic crystal properties. For example, it is not understood well in a good physical sense how delocalized electronic behavior associated with metal cations gives rise to paramagnetically shifted ^{29}Si and ^{27}Al NMR resonances (e.g., Palke et al. 2015). Low-temperature magnetic phase transitions in iron- and manganese-bearing silicate garnets are caused by different electronic super-exchange mechanisms that involve electron delocalization (e.g., Geiger et al. 2019). The magnetic transition behavior of end-member almandine has been analyzed computationally (Zhrebetskyy et al. 2012) and it is complex in detail. Photon-induced IVCT and associated electron delocalization in silicate garnet is also not understood in a precise physical sense, as this study shows. More focused and quantitative experimental investigations of electronic behavior are necessary. State-of-the-art ab-initio calculations could also possibly shed some light on these questions.

Finally, $\{Fe^{2+}\} + [Fe^{3+}] \rightarrow \{Fe^{3+}\} + [Fe^{2+}]$ IVCT in garnet can have a major effect on crystal color. More spectroscopic study on different garnet species and over a range of compositions is required to understand in a more quantitative sense the nature of their colors.

ACKNOWLEDGMENTS

545 J. Filip and A.B. Woodland provided almandine samples JF-1 and FR-3, respectively. O.A.
546 Vyshnevskyi kindly made several microprobe analyses. A. Locock provided helpful discussion on
547 garnet and R. Keene and D.M. D'Alessandro on IVCT behavior in various chemical systems. The
548 journal referees U. Hålenius and D. Dyar and the associate editor S. Redfern offered comments that
549 improved the manuscript. We thank them all. This research was supported by a grant to C.A.G.
550 from the Austrian Science Fund (FWF: P 30977-NBL). He also thanks the "Land Salzburg" for
551 financial support through the initiative "Wissenschafts- und Innovationsstrategie" Salzburg 2025".
552

REFERENCES CITED

Aparicio, C., Filip, J., Skogby, H., Marusak, Z., Mashlan, M., and Zboril, R. (2012) Thermal behavior of almandine at temperatures of 1,200 °C in hydrogen. Physics and Chemistry of Minerals, 39, 311-318.

Armbruster, T., and Geiger, C.A. (1993) Andradite crystal chemistry, dynamic X-site disorder and strain in silicate garnets. European Journal of Mineralogy, 5, 59-71.

Armbruster, T., Geiger, C.A., and Lager, G.A. (1992) Single crystal X-ray refinement of almandine pyrope garnets at 298 and 100 K. American Mineralogist, 77, 512-523.

Barker, F. (1964) Reaction between mafic magmas and pelitic schist, Cortlandt, New York. American Journal of Science, 262, 614-634.

Burns, R.G. (1981) Intervalence transitions in mixed-valence minerals of iron and titanium. Annual Review of Earth and Planetary Sciences, 9, 345-383.

Burns, R.G. (1993) Mineralogical Applications of Crystal Field Theory. Second edition. Cambridge University Press, Cambridge, England. 551 p.

Chakhmouradian, A.R., and McCammon, C.A. (2005) Schorlomite: a discussion of the crystal chemistry, formula, and inter-species boundaries. Physics and Chemistry of Minerals, 32, 277-289.

Cox, P.A. (1980) Electron transfer between exchange-coupled ions in mixed-valency compounds. Chemical Physics Letters, 69, 340-343.

Dorfler, K.M., Caddick, M.J., and Tracy, R.J. (2015) Thermodynamic modeling of crustal melting using xenolith analogs from the Cortlandt Complex, New York, USA. Journal of Petrology, 56, 389-408.

Dowty, E. (1971) Crystal chemistry of titantian and zirconian garnet: I. Review and spectral studies. American Mineralogist, 56, 1983-2009.

578 Geiger, C.A., and Armbruster, T. (1997) $Mn_3Al_2Si_3O_{12}$ spessartine and $Ca_3Al_2Si_3O_{12}$ grossular
579 garnet: dynamical structural and thermodynamic properties. American Mineralogist, 82,
580 740-747.
581 Geiger, C.A., and Taran, M.N. (Part IV - in prep.) On the color of hessonite.
582 Geiger, C.A., Taran, M.N. and Rossman, G.R. (in press) UV/Vis Single-Crystal Spectroscopic
583 Investigation of Almandine-Pyrope and Almandine-Spessartine Solid Solutions: Part I.
584 Spin-Forbidden $Fe^{2+,3+}$ and Mn^{2+} Electronic-Transition Energies, Crystal Chemistry and
585 Bonding Behavior. American Mineralogist.
586 Geiger, C.A., Grodzicki, M., and Dachs, E. (2019) An analysis of the magnetic behavior of olivine
587 and garnet substitutional solid solutions. American Mineralogist, 104, 1246-1255.
588 Girerd, J.J. (1983) Electron transfer between magnetic ions in mixed valence binuclear systems.
589 The Journal of Chemical Physics, 79, 1766-1775.
590 Gongbao, W., and Baolei, M. (1986) The crystal chemistry and Mössbauer study of schorlomite.
591 Physics and Chemistry of Minerals, 13, 198-205.
592 Grew, E.S., Locock, A.J., Mills, S.J., Galuskina, I.O., Galuskin, E.V., and Hålenius, U. (2013)
593 Nomenclature of the garnet supergroup. American Mineralogist, 98, 785-811.
594 Holwerda, R.A., Whittlesey, B.R., and Nilges, M.J. (1998) Crystal structure, physical properties,
595 and hydrolysis kinetics of $[(O)(tmpa)V^{IV}(\mu\text{-}O)V^{V}(tmpa)(O)]^{3+}$. Inorganic Chemistry, 37, 64-
596 68.
597 Huggins, F.E., Virgo, D., and Huckenholz, H.G., (1977a) Titanium-containing silicate garnets. I.
598 The distribution of Al, Fe^{3+}, and Ti^{4+} between octahedral and tetrahedral sites. American
599 Mineralogist, 62, 475-490.
600 Huggins, F.E., Virgo, D., and Huckenholz, H.G., (1977b) Titanium-containing silicate garnets. II.
601 The crystal chemistry of melanites and schorlomites. American Mineralogist, 62, 646-655.

602 Langer, K., Robarick, E., Sobolev, N.V., Shatsky, V.S., and Wang, W. (1993) Single-crystal spectra
603 of garnets from diamondiferous high-pressure metamorphic rocks from Kazakhstan:
604 indications for OH^-, H_2O, and FeTi charge transfer. European Journal of Mineralogy, 5,
605 1091-1100.
606 Laurs, B.M., and Knox, K. (2001) Spessartine garnet from Ramona, San Diego County, California.
607 Gems and Gemology, 37, no. 4, 278-295.
608 Locock, A.J. (2008) An Excel spreadsheet to recast analyses of garnet into end-member
609 components, and a synopsis of the crystal chemistry of natural silicate garnets. Computers
610 and Geoscience, 34, 1769-1780.
611 Locock, A., Luth, R.W., Cavell, R.G., Smith, D.G.W., and Duke, M.J.M. (1995) Spectroscopy of
612 the cation distribution in the schorlomite species of garnet. American Mineralogist, 80, 27-
613 38.
614 Manning, P.G. and Harris, D.C. (1970) Optical-absorption and electron-microprobe studies of some
615 high-Ti andradites. The Canadian Mineralogist, 10(2), 260-271.
616 Mattson, S.M., and Rossman, G.R. (1988) Fe^{2+}-Ti^{4+} charge transfer in stoichiometric Fe^{2+}, Ti^{4+}-
617 minerals. Physics and Chemistry of Minerals, 16, 78-82.
618 Moore, R.K. and White, W.B. (1971) Intervalence electron charge transfer effects in the spectra of
619 the melanite garnets. American Mineralogist, 56, 826-840.
620 Moore, R.K., and White, W.B. (1972) Electronic spectra of transition metal ions in silicate garnets.
621 Canadian Mineralogist, 11, 791-811.
622 Normand, C., and William-Jones, A.E. (2007) Physicochemical conditions and timing of rodingite
623 formation: evidence from rodingite-hosted fluid inclusions in the JM Asbestos mine,
624 Asbestos, Québec. Geochemical Transactions, 8.11, 1-19.
625 Novak, G.A., and Gibbs, G.V. (1971) The crystal chemistry of the silicate garnets. American
626 Mineralogist, 56, 791-825.

627 Palke, A.C., Stebbins, J.F., Geiger, C.A., and Tippelt, G. (2015) Cation order-disorder in Fe-bearing
628 pyrope and grossular garnets: An ^{27}Al and ^{29}Si MAS NMR and ^{57}Fe Mössbauer
629 spectroscopy study. American Mineralogist, 100, 536-547.
630 Platonov, A.N., Langer, K., Matsuk, S., Taran, M.N., and X. Hu. (1991) Fe^{2+}-Ti^{4+} charge-transfer in
631 garnets from mantle eclogites. European Journal of Mineralogy, 3, 19-26.
632 Schwartz, K.B., Nolet, D.A., and Burns, R.G. (1980) Mössbauer spectroscopy and crystal chemistry
633 of natural Fe-Ti garnets. American Mineralogist, 65, 142-153.
634 Sherman, D.M. (1987a) Molecular orbital (SCF-Xα-SW) theory of metal-metal charge transfer
635 processes in minerals. I. Application to Fe^{2+}-Fe^{3+} charge transfer and electron delocalization
636 in mixed-valence iron oxides and silicates. Physics and Chemistry of Minerals, 14, 355-363.
637 Sherman, D.M. (1987b) Molecular orbital (SCF-Xα-SW) theory of metal-metal charge transfer
638 processes in minerals. II. Application to $Fe^{2+} \rightarrow Ti^{4+}$ charge transfer transitions in oxides
639 and silicates. Physics and Chemistry of Minerals, 14, 364-367
640 Souček, J. (1978) Metamorphic zones of the Vrbno and Rejvíz Series, the Hrubý Jeseník
641 Mountains, Czechoslovakia. Tschermaks Mineralogische und Petrographische Mitteilungen,
642 25, 195-217.
643 Spetsius, Z.V., and Serenko, V.P. (1990) Composition of continental upper mantle and lower crust
644 beneath the Siberian platform. Nauka Publishing House, Moscow (in Russian), USSR, 272
645 p.
646 Suzuki, M., Fujinami, S., Hibino, T., Hori, H., Maeda, Y., Uehara, A., and Suzuki, M. (1998)
647 Synthesis and characterization of mixed valence μ-alkoxo-diiron (II,III) complexes with an
648 unsymmetric dinucleating ligand. Inorganica Chimica Acta, 283, 124-135.
649 Taran, M.N., Dyar, M.D., and Matsuyk, S.S. (2007) Optical absorption study of natural garnets of
650 almandine-skiagite composition showing intervalence $Fe^{2+} + Fe^{3+} \rightarrow Fe^{3+} + Fe^{2+}$ charge-
651 transfer transition. American Mineralogist, 92, 753-760.

652 Taran, M.N., Geiger, C.A., and Vyshnevskyi, O.A. (in prep.) “Little ember of coal”: Part IV. The
653 color of almandine and almandine-bearing garnets. American Mineralogist.
654 Taran, M.N., Geiger, C.A., Vyshnevskyi, O.A., and Rossman, G.R. (in press) Single-crystal
655 UV/Vis Optical Absorption Spectra of Almandine-Bearing and Spessartine Garnet: Part II.
656 An Analysis of the Spin-Forbidden Bands of Fe^{2+}, Mn^{2+}, and Fe^{3+}. American Mineralogist.
657 Wong, K.Y., Schatz, P.N., and Piepho, S.B. (1979) Vibronic coupling model for mixed-valence
658 compounds. Comparisons and predictions. Journal of the American Chemical Society, 101,
659 2793-2803.
660 Woodland, A.B., Droop, G., and O’Neill, H.St.C. (1995) Almandine-rich garnet from near
661 Collobrieres, southern France, and its petrological significance. European Journal of
662 Mineralogy, 7, 187-194.
663 Zhrebetskyy, D., Lebernegg, S., Amthauer, G., and Grodzicki, M. (2012) Magnetic structure of
664 almandine. Physics and Chemistry of Minerals, 39, 351-361.

665

666 Table 1. Description of garnet samples.

Species and Label	Locality	Occurrence and Description
Alm - FR-3	near Collobrières, France	Metamorphosed ironstone. Studied by Woodland et al. (1995) and Dachs et al. (2012).
Alm - JF-1	Zlaty Chlum near Jesenik, Czech Republic	Brownish red crystal studied by Aparicio et al. (2012). From a regionally metamorphosed terrane (Souček (1978).
Alm-(Pyp) - GRF 90-33	De Luca Pit, Emery Hill, Corlandt, N.Y., USA	In metamorphic hornfels. Described in Taran et al. (2007) and Dorfler et al. (2015).
Sps - 316306	Africa?	Platelet made from a vivid red facetted crystal. Described in Taran et al. (in press). From ThaiGemStore, ebay.
Sps - 200924241653	Nigeria	Platelet made from a dark brownish red polished cabochon. From nngems, ebay.
Grs - SGM-1	Sri Lanka	Platelet made from an orange red facetted stone. Hessonite. From SiamGemsMart, ebay.
Grs - GR 10074	Jeffrey Mine, Asbestos, Quebec, Canada	Occurs in a rodingite. Reddish brown doubly polished thick crystal block. Described in Palke et al. (2015).

667
668
669
670
671
672
673

Table 2a. Compositions of the measured garnets in terms of oxides from this study (i.e., SGM-1) and taken from Geiger et al. (Part I - in press) and the literature as noted. The totals of 316306, 200924241653 and SGM-1 are normalized to 100.00.

Oxides	SGM-1	316306[⊗]	200924241653[⊗]	FR-3[§]	JF-1[#]
SiO_2	39.52	36.71	36.44	37.22	36.09
TiO_2	0.33	0.10	0.13	0.02	0.04
Al_2O_3	21.84	20.52	20.50	20.34	20.44
Cr_2O_3	-	-	-	-	0.01
FeO	3.62	7.17	12.50	43.29	41.19
MnO	0.09	33.24	29.96	0.05	0.21
MgO	0.17	1.21	-	0.61	0.91
CaO	34.42	1.04	0.48	1.04	0.56
Total	100.00	100.00	100.00	102.57	99.45

Taken from [⊗]Geiger et al. (Part I - in press), [§]Dachs et al. (2012) and [#]Aparicio et al. (2012).

This is the peer-reviewed, final accepted version for American Mineralogist, published by the Mineralogical Society of America.
The published version is subject to change. Cite as Authors (Year) Title. American Mineralogist, in press.
DOI: https://doi.org/10.2138/am-2022-8756. http://www.minsocam.org/

682 Table 2b. Crystal chemical formulas of the studied garnets expressed in terms of various end-member garnet components in percent
683 following Locock (2008). The data for the calculations come from this study, Geiger et al. (Part I - in press and Table 2a) and the
684 literature (GT 90-33 and GR-10074, which is not calculated using Locock 2008). Remainder is the difference from 100.0% and could
685 not be assigned. The calculated Fe^{3+}/Fe^{tot} ratio is given in percent below.

End-Member	Formula	FR-3	JF-1	GT 90-33#	316306	200924-241653	SGM-1	GR-10074§
Schorlomite-Al	$\{Ca_3\}[Ti_2](SiAl_2)O_{12}$	0.06	0.12	0.45	0.22	-	0.51	-
Morimotoite	$\{Ca_3\}[TiFe_2](SiAl_2)O_{12}$	-	-	-	0.17	-	0.86	-
Uvarovite	$\{Ca_3\}[Cr_2](Si_3)O_{12}$	-	0.03	0.09	-	-	-	-
Spessartine	$\{Mn_3\}[Al_2](Si_3)O_{12}$	0.11	0.49	2.02	76.58	69.73	0.19	-
Pyrope	$\{Mg_3\}[Al_2](Si_3)O_{12}$	2.44	3.74	44.32	4.91	-	0.64	-
Almandine	$\{Fe_3\}[Al_2](Si_3)O_{12}$	93.50	93.62	46.28	15.48	28.73	6.17	2.4
Grossular	$\{Ca_3\}[Al_2](Si_3)O_{12}$	-	0.83	3.49	1.48	1.13	89.86	96.7
Andradite	$\{Ca_3\}[Fe_2](Si_3)O_{12}$	2.93	0.67	2.60	1.16	-	1.77	0.4
Skiagite	$\{Fe_3\}[Fe_2](Si_3)O_{12}$	0.77	-	-	-	-	-	-
Remainder	-	0.18	0.50	0.75	0.0	0.41	0.0	-
Total		99.99	100.00	100.00	100.00	100.00	100.00	99.14
Fe^{3+}/Fe^{tot}		2.86	1.34	6.06	4.73	0.00	15.47	7.4

686 Taken directly from §Palke et al. (2015). Calculated using the oxide weight percent values given in #Taran et al. (2007).

This is the peer-reviewed, final accepted version for American Mineralogist, published by the Mineralogical Society of America.
The published version is subject to change. Cite as Authors (Year) Title. American Mineralogist, in press.
DOI: https://doi.org/10.2138/am-2022-8756. http://www.minsocam.org/

687 Table 3. Crystal-chemical formulas of the garnets studied by Taran et al. (2007) and the one sample (257) of Langer et al. (1993) expressed in
688 terms of various garnet end-member components in percent following Locock (2008). Remainder means cannot be assigned. The calculated atomic
689 Fe^{3+}/Fe^{tot} ratio is given in percent below.

End-Member	Formula	GTF 90-28	SM 1348	WGR 1R	GT 90-33	UEP-1/77	2152	YuK-371/77	257 (1)
Schorlomite-Al	$\{Ca_3\}[Ti^{4+}_2](SiAl_2)O_{12}$	0.06	0.14	0.08	0.45	0.26	0.35	0.66	-
Morimotoite	$\{Ca_3\}[TiFe](Si_3)O_{12}$	-	-	-	-	-	-	-	1.69
Uvarovite	$\{Ca_3\}[Cr^{3+}_2](Si_3)O_{12}$	0.12	0.06	0.12	0.09	-	0.06	0.41	-
Majorite	$\{Mg_3\}[SiMg](Si_3)O_{12}$	-	-	-	-	-	-	-	0.58
Spessartine	$\{Mn^{2+}_3\}[Al_2](Si_3)O_{12}$	1.80	0.92	1.51	2.02	1.22	1.32	2.79	5.09
Pyrope	$\{Mg_3\}[Al_2](Si_3)O_{12}$	22.57	42.63	37.00	44.32	26.93	25.13	19.66	24.89
Almandine	$\{Fe^{2+}_3\}[Al_2](Si_3)O_{12}$	70.34	41.60	42.57	46.28	56.02	54.26	59.92	48.75
Grossular	$\{Ca_3\}[Al_2](Si_3)O_{12}$	3.14	11.26	16.64	3.49	11.87	13.71	11.66	18.17
Andradite	$\{Ca_3\}[Fe^{3+}_2](Si_3)O_{12}$	1.37	2.27	1.67	2.60	2.97	4.41	3.63	0.82
Skiagite	$\{Fe^{2+}_3\}[Fe^{3+}_2](Si_3)O_{12}$	-	-	-	-	-	-	-	-
Remainder	-	0.21	1.12	0.42	0.75	0.73	0.76	1.27	0.00
Total		100.01	100.0	100.0	100.0	100.0	100.0	100.0	99.99
Fe^{3+}/Fe^{tot}		2.67	7.50	4.09	6.06	5.41	7.21	7.04	1.10

This is the peer-reviewed, final accepted version for American Mineralogist, published by the Mineralogical Society of America.
The published version is subject to change. Cite as Authors (Year) Title. American Mineralogist, in press.
DOI: https://doi.org/10.2138/am-2022-8756. http://www.minsocam.org/

690

691 Table 4. IVCT exchange mechanisms and their energies proposed for silicate garnet of general formula $\{X_3\}[Y_2](Z_3)O_{12}$ (see text for

692 discussion).

IVCT Mechanism	Energy (cm^{-1})	Ca-Ti-bearing Garnets	Aluminosilicate Garnets
$\{Fe^{2+}\} + [Ti^{4+}] \rightarrow \{Fe^{3+}\} + [Ti^{3+}]$[1, 2]	23500[1], 23457[1, this study] 21500[2], 22270[2, this study]	-	yes
$[Ti^{4+}] + (Fe^{2+}) \rightarrow [Ti^{3+}] + (Fe^{3+})$[3]	~20000	yes	-
"$\{Fe^{2+}\} + (Fe^{3+}) \rightarrow \{Fe^{3+}\} + (Fe^{2+})$"[4]	~5280	questionable	-
$[Fe^{2+}] + (Fe^{3+}) \rightarrow [Fe^{3+}] + (Fe^{2+})$[3]	?	possibly	-
$\{Fe^{2+}\} + [Fe^{3+}] \rightarrow \{Fe^{3+}\} + [Fe^{2+}]$[5, this study]	~21700[5], 21000-22000[this study]	-	yes

693

694 [1]Platonov et al. (1991), [2]Langer et al (1993), [3]Locock et al. (1995), [4]Moore and White (1972) and Schwartz et al. (1980), [5]Taran et al.

695 (2007). The mechanism "$\{Fe^{2+}\} + (Fe^{3+}) \rightarrow \{Fe^{3+}\} + (Fe^{2+})$" was questioned by Locock et al. (1995). The proposal of $\{Fe^{2+}\} + [Ti^{4+}] \rightarrow$

696 $\{Fe^{3+}\} + [Ti^{3+}]$ IVCT in the garnets investigated by Langer et al. (1993) is discussed in the text.

697

698

This is the peer-reviewed, final accepted version for American Mineralogist, published by the Mineralogical Society of America.
The published version is subject to change. Cite as Authors (Year) Title. American Mineralogist, in press.
DOI: https://doi.org/10.2138/am-2022-8756. http://www.minsocam.org/

Figures

Fig. 1. Spectra of two nearly end-member almandines FR-3 (a) and JF-1 (b) with compositions $\{Fe^{2+}_{2.83}Mg_{0.07}Ca_{0.09}\}[Al_{1.92}Fe^{3+}_{0.08}]Si_{2.99}O_{12}$ and $\{Fe^{2+}_{2.85}Mg_{0.11}Mn^{2+}_{0.02}Ca_{0.05}\}[Al_{1.99}]Si_{2.99}O_{12}$, respectively. The experimental spectra are shown by dotted lines. The total spectral fit is given by the red line and the individual bands are shown below by the black lines (see Supplementary Tables 1 and 2). The absorption spectra are dominated by an intense $\{Fe^{2+}\} + [Fe^{3+}] \rightarrow \{Fe^{3+}\} + [Fe^{2+}]$ IVCT band centered at roughly 21500 cm^{-1}. The narrow l, m and the relatively intense r band are caused by electronic Fe^{3+} spin-forbidden transitions. They and the other Fe^{2+} and Fe^{3+} spin-forbidden bands are discussed in Taran et al. (Part II – in press). The band ?? is not observed in the experimental spectrum, but is necessary to obtain a satisfactory fit to the spectrum. It may possibly be caused by the electronic spin-forbidden transition $^6A_{2g} \rightarrow {}^4T_{2g}$ (^4D) of $[Fe^{3+}]$.

Fig. 2. Spectrum of an intermediate almandine-pyrope solid-solution, GTF 90-33, of composition $\{Fe^{2+}_{1.39}Mg_{1.33}Mn^{2+}_{0.06}Ca_{0.20}\}[Al_{1.92}Fe^{3+}_{0.09}](Si_{2.97}Al_{0.03})O_{12}$, as shown by the dotted line. The total spectral fit is given by the red line and the individual bands are shown below (see also Supplementary Table 3). The broad $\{Fe^{2+}\} + [Fe^{3+}] \rightarrow \{Fe^{3+}\} + [Fe^{2+}]$ IVCT band is centered at about 21718 cm^{-1}. The relatively intense narrow band r is a Fe^{3+} spin-forbidden transition. It and the other Fe^{2+} and Fe^{3+} spin-forbidden bands are discussed in Taran et al. (Part II – in press). The bands ? and ?? are not observed in the experimental spectrum, but they are necessary to obtain a satisfactory fit to the spectrum. The latter may possibly be caused by the electronic spin-forbidden transition $^6A_{2g} \rightarrow {}^4T_{2g}$ (^4D) of $[Fe^{3+}]$.

Fig. 3. Spectra of two spessartines 316306 (a) and 200924241653 (b) with compositions $\{Mn^{2+}_{2.30}Fe^{2+}_{0.47}Mg_{0.15}Ca_{0.09}\}[Al_{1.97}Fe^{3+}_{0.02}]Si3_{.00}O_{12}$ and $\{Mn^{2+}_{2.09}Fe^{2+}_{0.86}Ca_{0.04}\}[Al_{1.99}]Si_{3.00}O_{12}$, respectively. The experimental spectra are shown by the dotted lines. The total spectral fits are given by the red lines and the individual bands are shown below (see Supplementary Tables 4 and 5). The broad band with a maximum between 20500 and 21000 cm^{-1} is assigned to an electronic $\{Fe^{2+}\} + [Fe^{3+}] \rightarrow \{Fe^{3+}\} + [Fe^{2+}]$ IVCT. The weaker and narrower bands p, o, n and n' located between 22000 and 25000 cm^{-1} are various spin-forbidden bands of $^{VIII}Mn^{2+}$ (see Taran et al. Part II – in press). Their deviation from pure Gaussian shape in the deconvolution is related to the fitting procedure.

Fig. 4. Spectra of two grossulars SGM-1 (a) and GR 10074 (b) with compositions $\{Ca_{2.79}Fe^{2+}_{0.19}Mg_{0.02}Mn^{2+}_{0.01}\}[Al_{1.95}Fe^{3+}_{0.04}Ti^{4+}_{0.02}](Si_{2.99})O_{12}$ and $\{Ca_{2.89}Fe^{2+}_{0.09}Mn^{2+}_{0.03}\}[Al_{1.96}Fe^{3+}_{0.01}](Si_{3.00})O_{12}$, respectively. The experimental spectra are shown by the dotted lines. The total spectral fits are given by the red lines and the individual fit bands are shown below (see Supplementary Tables 6 and 7). The broad band with a maximum at about 22700 cm^{-1} (SGM-1) and 21200 cm^{-1} (GR 10074) is assigned to an electronic $\{Fe^{2+}\} + [Fe^{3+}] \rightarrow \{Fe^{3+}\} + [Fe^{2+}]$ IVCT. The weaker and narrower bands p, n and n′ located between 2300 and 25000 cm^{-1} are spin-forbidden bands of $^{VIII}Mn^{2+}$ (see Taran et al. Part II – in press). The weak bands located at lower wavenumbers are spin-forbidden bands of $\{Fe^{2+}\}$. The relatively intense band r in both spectra at about 27000 cm^{-1} is a Fe^{3+} spin-forbidden transition.

Fig. 5. ^{57}Fe Mössbauer spectrum of grossular, GR 10074. The fit gives two doublets, a stronger one (red) with an isomer shift of 1.27 mm/sec and a quadrupole splitting of 3.54 mm/sec and a weaker one (blue) with an isomer shift of 0.51 mm/sec and quadrupole splitting of 0.56 mm/sec. The former doublet corresponds to $\{Fe^{2+}\}$ and the latter to $[Fe^{3+}]$.

Fig. 6. Comparison of the various fitted IVCT bands taken from the spectra of the garnets studied in this work. Note that the band intensity maximum for SGM-1 falls at higher wavenumbers compared to those of the other garnets.

This is the peer-reviewed, final accepted version for American Mineralogist, published by the Mineralogical Society of America.
The published version is subject to change. Cite as Authors (Year) Title. American Mineralogist, in press.
DOI: https://doi.org/10.2138/am-2022-8756. http://www.minsocam.org/

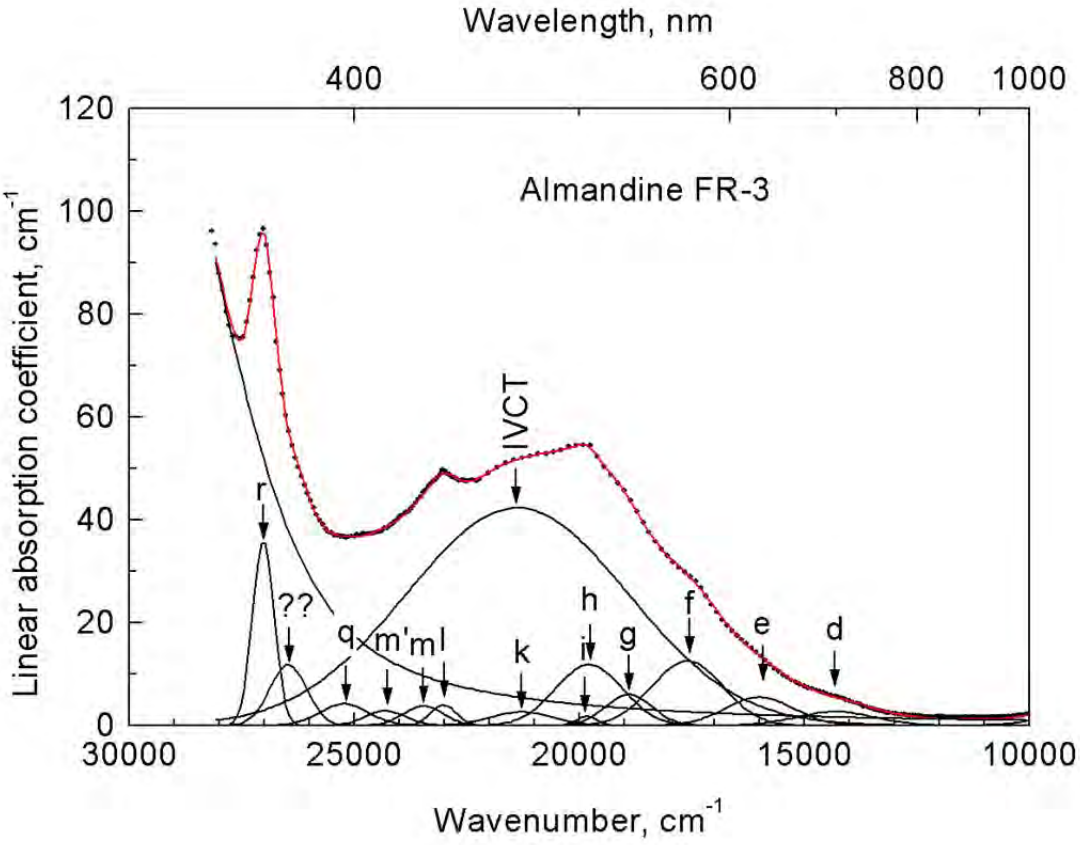

1a.

This is the peer-reviewed, final accepted version for American Mineralogist, published by the Mineralogical Society of America.
The published version is subject to change. Cite as Authors (Year) Title. American Mineralogist, in press.
DOI: https://doi.org/10.2138/am-2022-8756. http://www.minsocam.org/

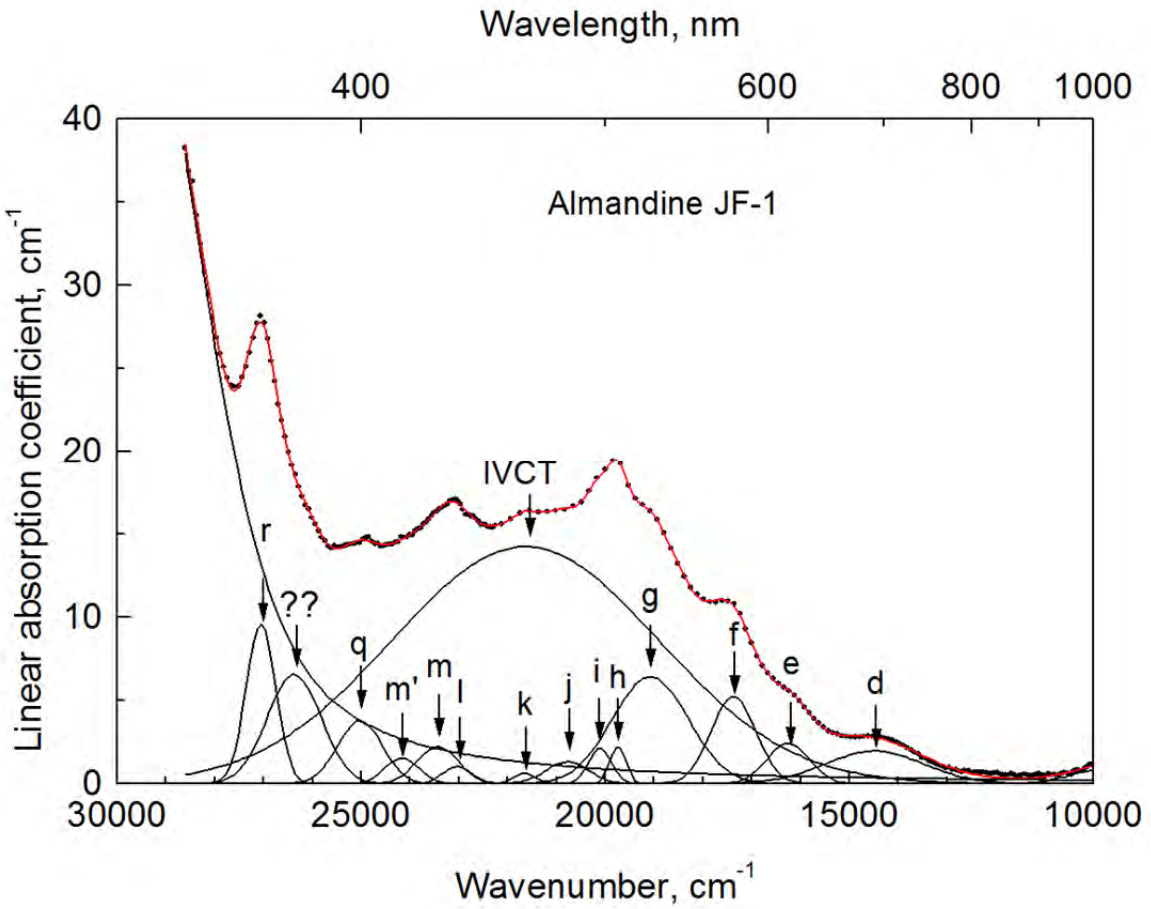

1b.

Figure 1.

999

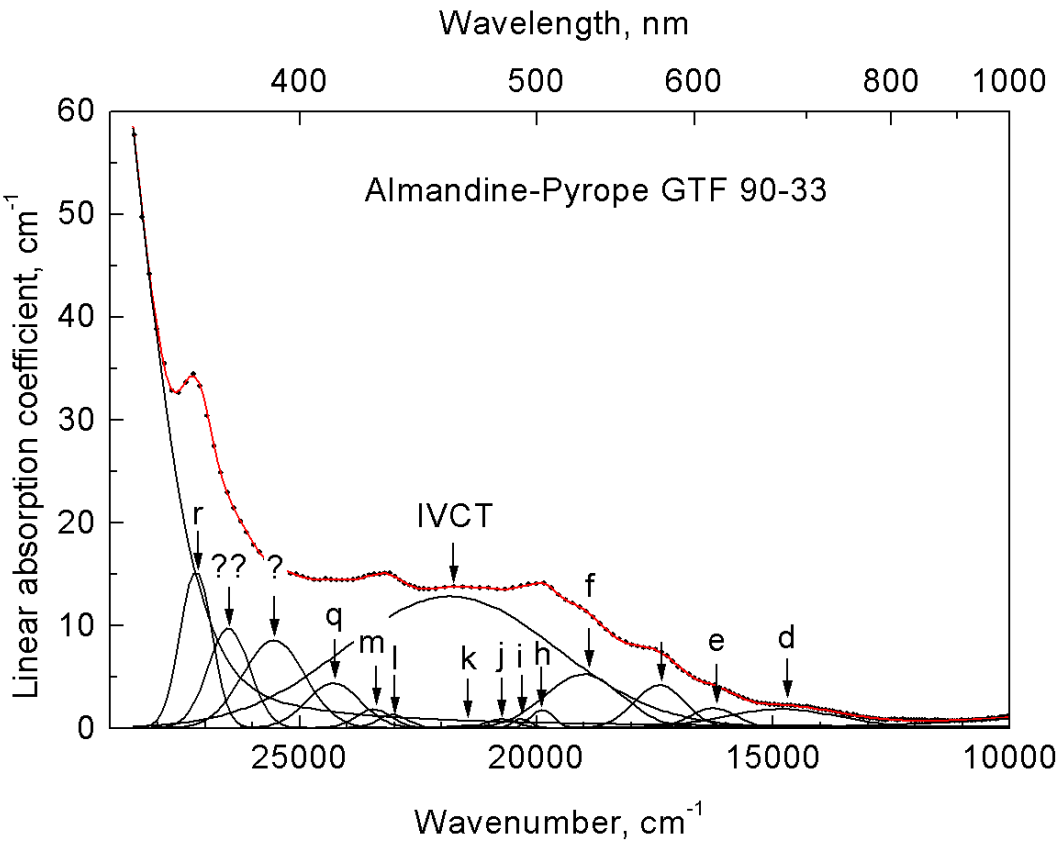

1000

1001

1002

1003

1004 Figure 2.

1005

1006

1007

1008

1009

1010

1011

1012

This is the peer-reviewed, final accepted version for American Mineralogist, published by the Mineralogical Society of America.
The published version is subject to change. Cite as Authors (Year) Title. American Mineralogist, in press.
DOI: https://doi.org/10.2138/am-2022-8756. http://www.minsocam.org/

1013

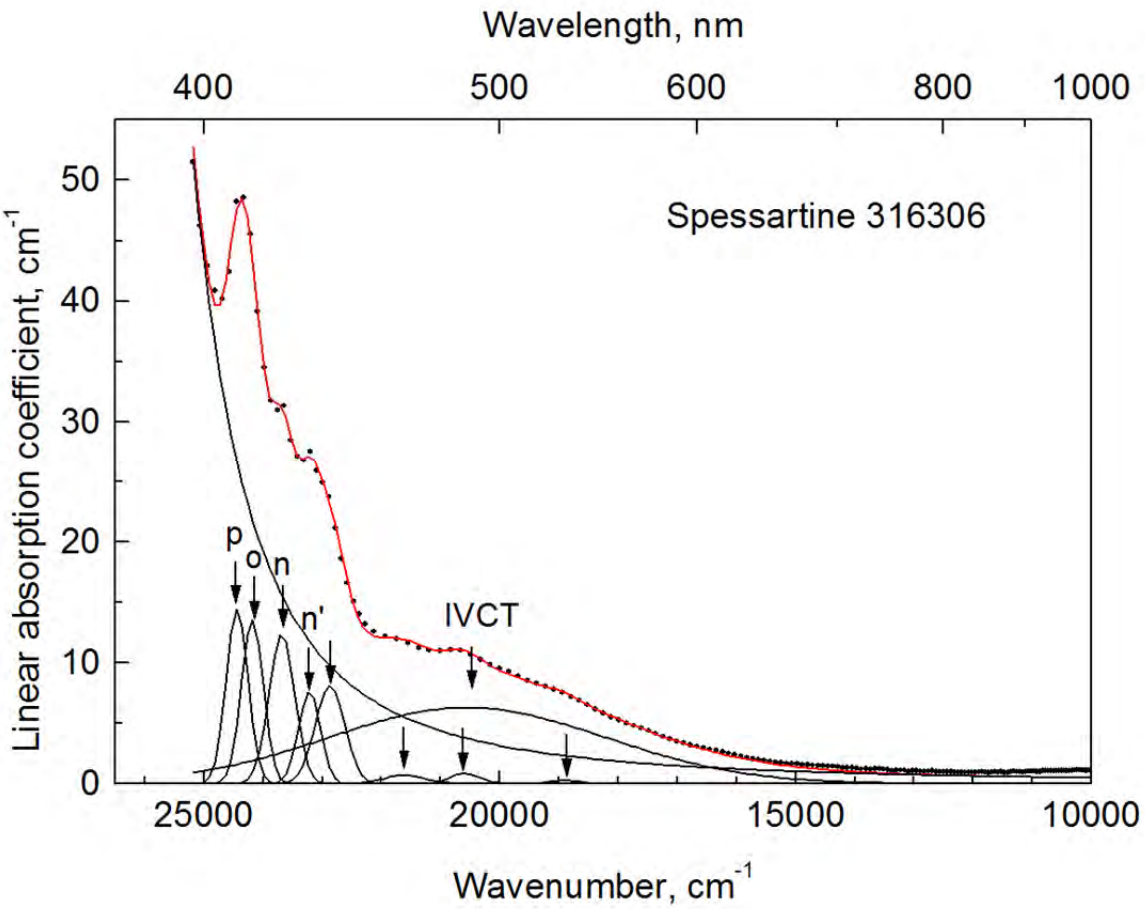

1014
1015
1016
1017 3a.
1018
1019
1020
1021
1022
1023
1024
1025
1026
1027
1028
1029
1030
1031
1032
1033
1034
1035
1036

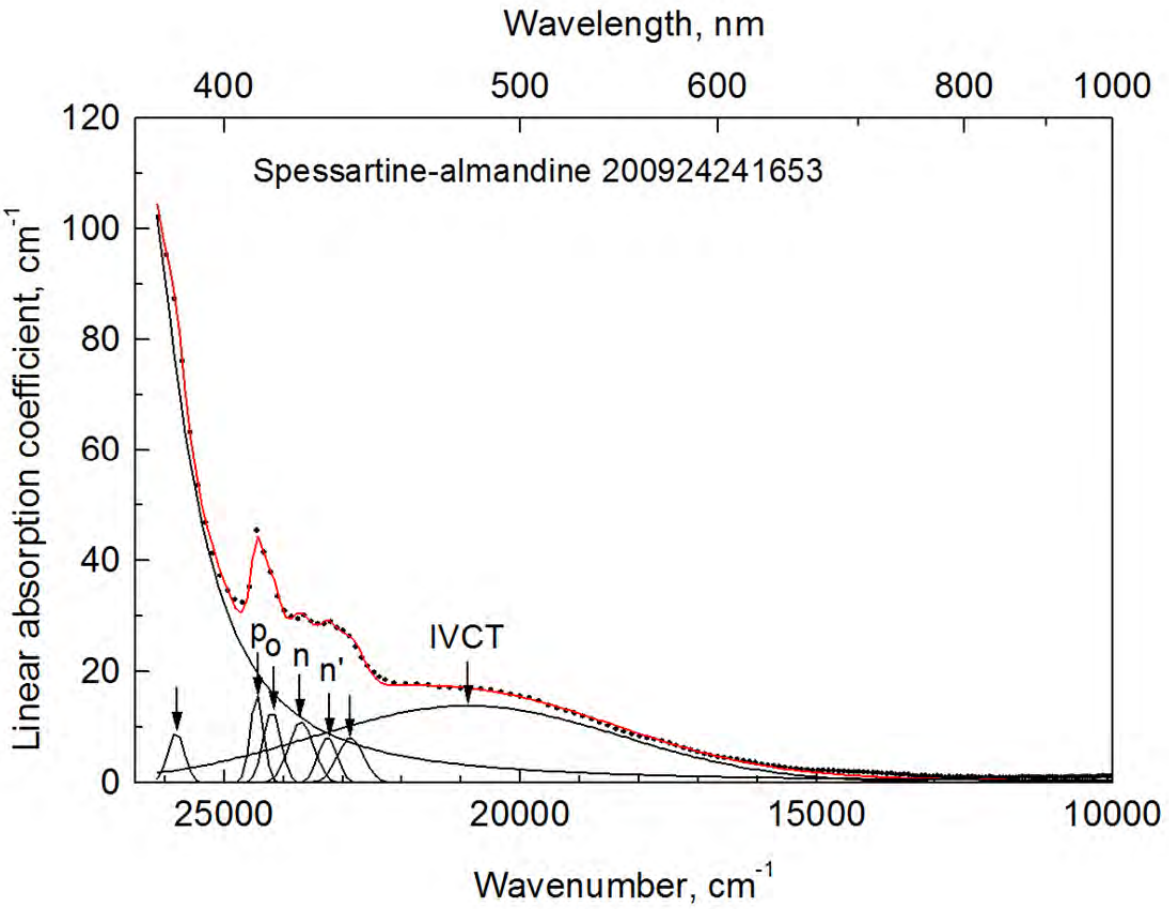

3b.

Figure 3.

This is the peer-reviewed, final accepted version for American Mineralogist, published by the Mineralogical Society of America.
The published version is subject to change. Cite as Authors (Year) Title. American Mineralogist, in press.
DOI: https://doi.org/10.2138/am-2022-8756. http://www.minsocam.org/

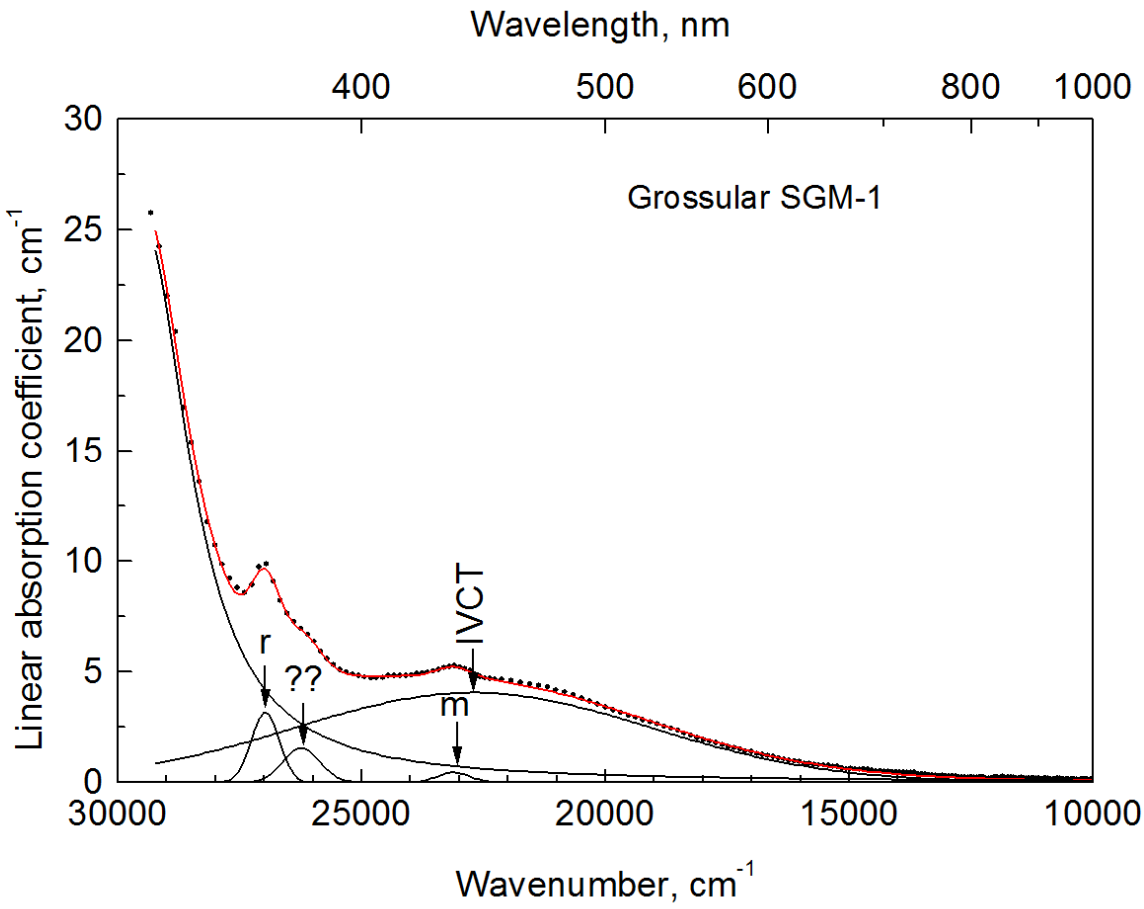

4a.

This is the peer-reviewed, final accepted version for American Mineralogist, published by the Mineralogical Society of America.
The published version is subject to change. Cite as Authors (Year) Title. American Mineralogist, in press.
DOI: https://doi.org/10.2138/am-2022-8756. http://www.minsocam.org/

1068

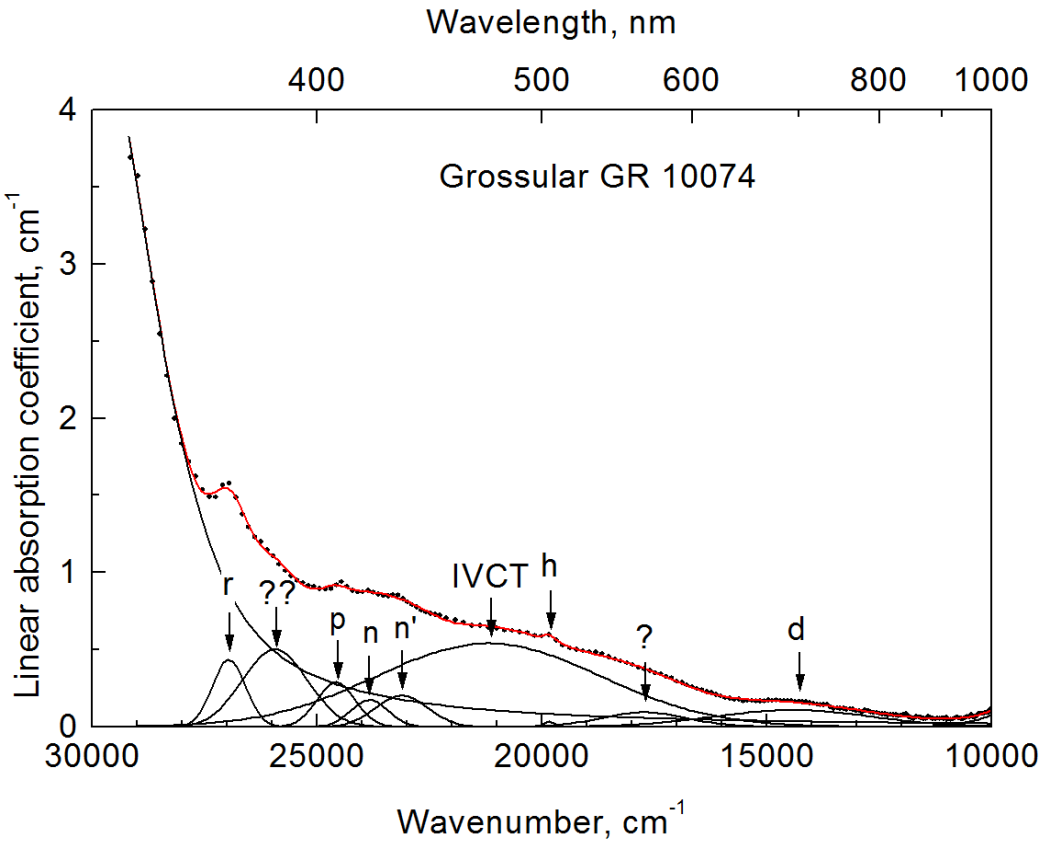

1069

1070

1071 4b.

1072

1073

1074 Figure 4.

1075

1076

1077

1078

1079

1080

This is the peer-reviewed, final accepted version for American Mineralogist, published by the Mineralogical Society of America.
The published version is subject to change. Cite as Authors (Year) Title. American Mineralogist, in press.
DOI: https://doi.org/10.2138/am-2022-8756. http://www.minsocam.org/

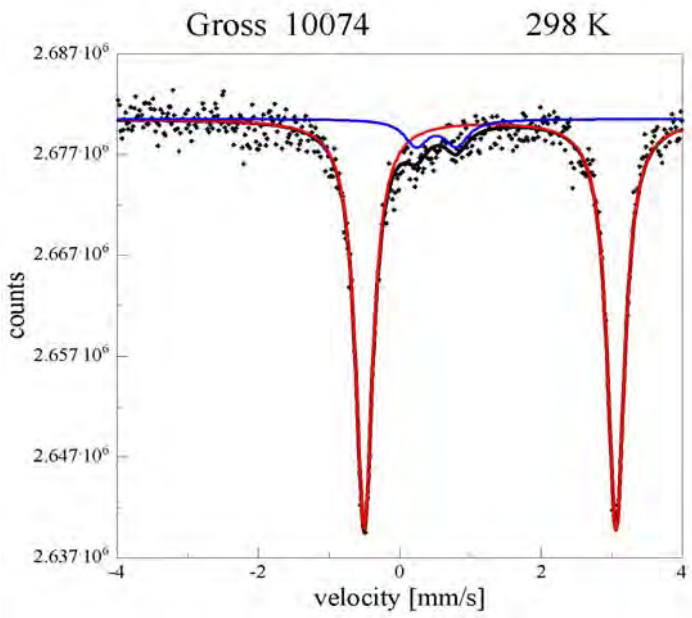

Figure 5.

This is the peer-reviewed, final accepted version for American Mineralogist, published by the Mineralogical Society of America.
The published version is subject to change. Cite as Authors (Year) Title. American Mineralogist, in press.
DOI: https://doi.org/10.2138/am-2022-8756. http://www.minsocam.org/

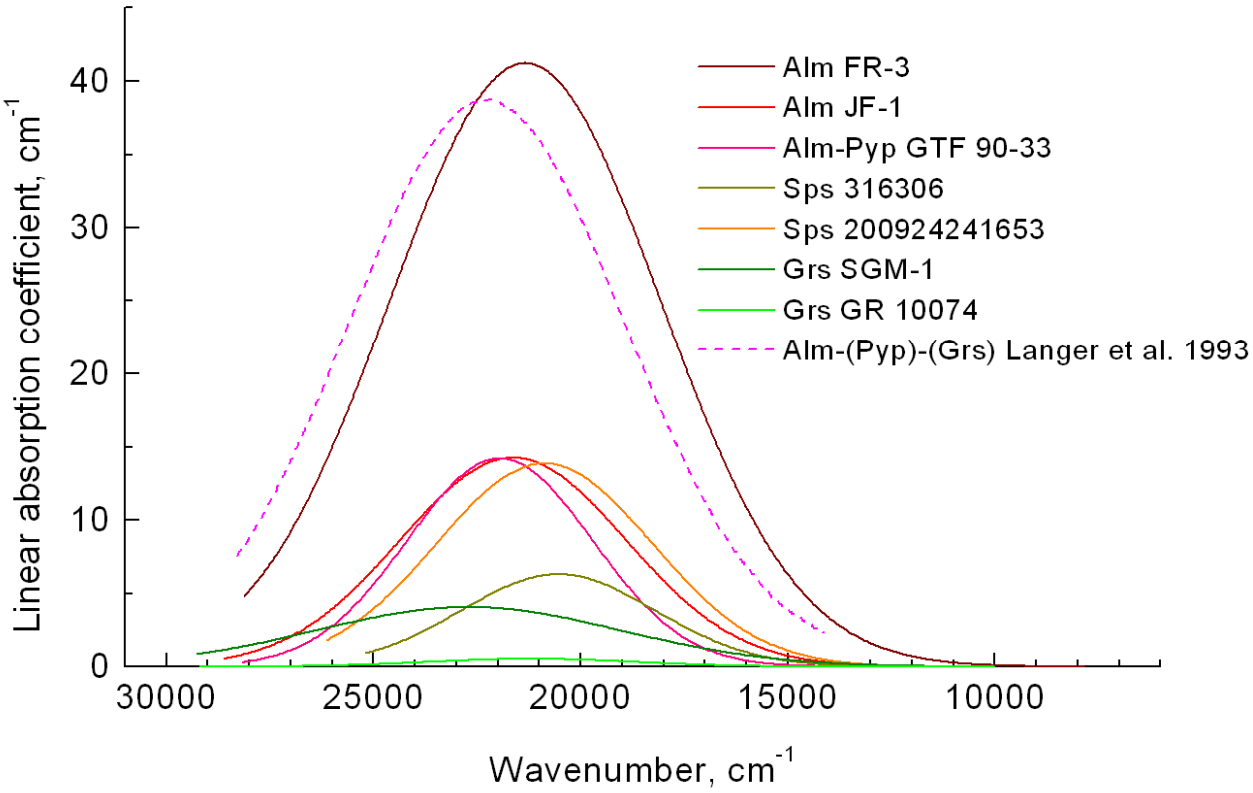

Fig. 6